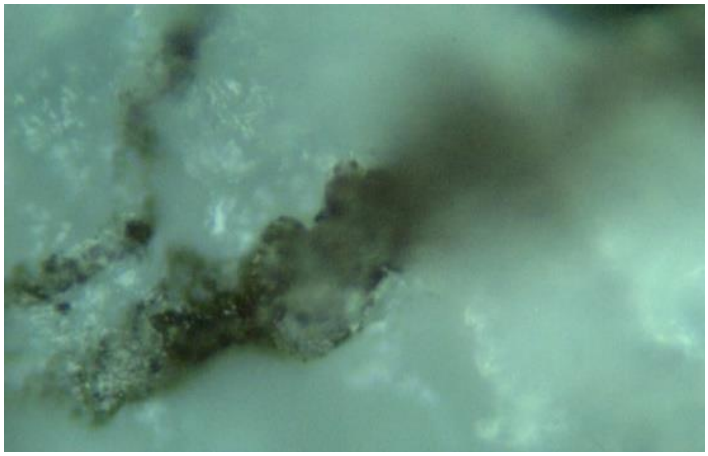

Raman Spectroscopy in tumoral tissues

João Manuel Ribeiro Jordão

Mestrado em Física Médica

Departamento de Física e Astronomia

2018/2019

Orientador

Orlando José Reis Frazão, Professor Auxiliar Convidado

Faculdade de Ciências, Universidade do Porto

Coorientador

Susana Ferreira de Oliveira Silva, Investigadora

INESC-TEC, Universidade do Porto

Todas as correções determinadas

pelo júri, e só essas, foram efetuadas.

O Presidente do Júri,

Porto, _____/_____/_____

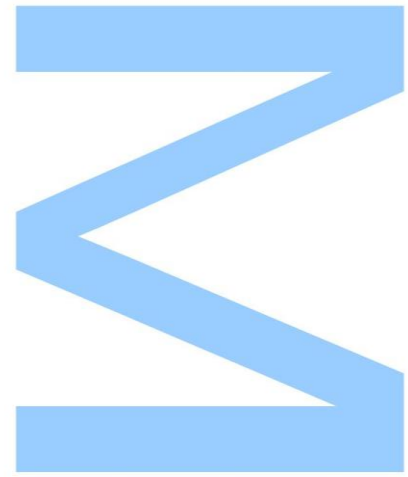

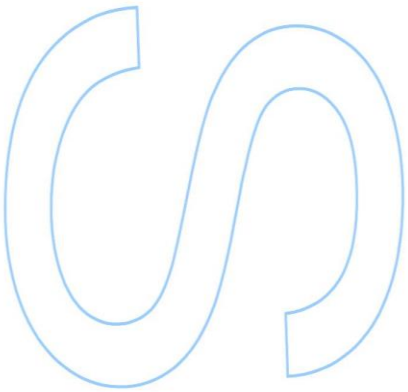

Dedicatória

Aos meus pais, João e Paula, sem eles eu nunca seria nada.

Ao meu irmão por todo o carinho e preocupação.

À Elisabete, que foi um grande apoio nestes anos.

A todos um obrigado por estarem presentes.

“Without love it cannot be seen…”

Ryukishi07, Umineko no Naku Koro ni

Agradecimentos

Ao meu orientador, Orlando José Reis Frazão, e coorientadora, Susana Ferreira Oliveira Silva, por me terem aceitado para este trabalho. Em conjunto com a Susana Novais, a sua ajuda foi crucial que me levou a melhorar como aluno e trabalhador com boas práticas de pesquisa, escrita e espírito crítico em conjunto com uso de novas ferramentas. Foi preponderante o seu contributo para uma dissertação bem conseguida.

Ao professor Joaquim Agostinho Moreira, por me ter ajudado numa altura menos feliz, ter acreditado e dado uma oportunidade para singrar.

A Rui Vilarinho por toda a ajuda em tudo que envolvesse espectroscopia de Raman, desde a aquisição de dados à validação da análise dos mesmos.

A Luísa Mendonça pela contínua boa disposição e simpatia.

A todos também um grande obrigado pela paciência e profissionalismo com que fui apresentado ao longo destes anos.

Um agradecimento ao INESC-TEC CAP, IFIMUP e Universidade do Porto pelos laboratórios e equipamento disponibilizado.

Agradeço também ao Hospital Veterinário de Évora e à professora Joana Reis pela ajuda e fornecimento de amostras.

Abstract

According to data of 2018 from the World Health Organisation (WHO), female breast and stomach cancers are the second and fifth types of cancers, respectively, in regards of new cases (close to 2.1 and 1.0 million new cases each); and are fifth and third when speaking of mortality rate (627 and 783 thousand for each).

Thus, pushing the need for new improved methods of either therapy or, preferably, diagnostic. Having an early diagnosis reduces the mortality rate of the patient.

With the aim of improving cancer diagnosis schemes this dissertation work researches the usage of Raman spectroscopy to detect traces of cancer tissues in samples.

Firstly, a research of the Raman effect was done to better understand the process and its limitations. Afterwards a literature review was done on the usage of Raman spectroscopy applied to both mammary and digestive tract tissues to help visualize the current state of the art, the best practices of the technique in biological samples and the kind of data one would be able to expect.

Human tissue samples acquirement can be a lengthy process. Research was done to check if there is a correlation or even better, a way to translate the results obtained using a household pet to human cancer. Which was determined to be doable.

Because of this fact, feline mammary tissue was analysed using the present Raman spectroscopy equipment determining the presence of four different types of spectra on the samples that were attributed to four different tissues. Two of them being believed to be a benign and malign tumour tissues.

***Key Words*:** Raman effect, Raman spectroscopy, mammary tissue, digestive tract, cancer, fibre optics, micro structured optical fibres

Resumo

De acordo com dados de 2018 da Organização Mundial de Saúde (WHO), os cancros da mama e de estômago são os segundos e quintos tipos de cancro, respetivamente, em termos de novos casos (aproximadamente 2.1 e 1.0 milhões cada), e são quinto e terceiro quando falando de taxa de mortalidade (627 e 783 mil cada um).

Portanto, criando a necessidade de desenvolver novos ou melhorados métodos de terapia ou, preferencialmente, diagnóstico, conseguindo um diagnóstico atempado, reduzindo a taxa de mortalidade do paciente.

Com o objetivo de melhorar os esquemas de diagnóstico de cancro este trabalho de dissertação pesquisa o uso de espectroscopia de Raman para detetar traços de tecidos cancerígenos em amostras.

Primeiramente, a pesquisa do efeito Raman foi feita para melhor entender o processo e as suas limitações. Após isso uma revisão de literatura foi feita no uso da espectroscopia de Raman aplicada a tanto tecidos mamários como do trato digestivo para ajudar a visualizar o corrente estado de arte, as boas práticas da técnica em amostras biológicas e que tipo de dados se poderia esperar obter.

Obter amostras de tecido humano pode ser um processo moroso. Pesquisa foi feita para averiguar se existe uma correlação ou melhor uma maneira de transladar os resultados obtidos usando um animal doméstico para cancro humano. O que foi determinado como fazível.

Devido a este facto, foi analisado tecido mamário felino usando o equipamento de espectroscopia de Raman presente. Nele foi determinado a presença de quatro espectros diferentes que foram atribuídos a quatro tecidos diferentes. Dos quais dois acreditasse serem tecidos tumorais benigno e maligno.

***Palavras-chave*:** Efeito Raman. espectroscopia Raman, tecido mamário, trato digestivo, cancro, fibras óticas, fibras óticas micro estruturadas.

Contents

Figure Index

Table index

Acronyms

WHO	World Health Organization
CARS	Coherent anti-Stokes Raman scattering
SRS	Stimulated Raman scattering
CRS	Coherent Raman scattering
NIR-RS	Near infrared Raman spectroscopy
HW-RS	High wavenumber Raman spectroscopy
LDA	Linear discriminant analysis
PCA	Principal component analysis
CCD	Charge coupled device
PCF	Photonic crystal fibres
HC-PCF	Hollow core photonic crystal fibres
PBG	Photonic bandgap guiding

Chapter 1 – Introduction and Motivation

1. Introduction

In 1930 Sir Chandrasekhara Venkata Raman won the Nobel prize in Physics by describing what is now called the Raman effect. Using an analogy with X-ray scattering the article describes the effect as being a new type of secondary radiation [1].

Raman effect is a second order scattering process [2, 3]. When a photon collides with the sample it might either lose energy (called a Stokes shift) or gain energy (anti-Stokes shift). The coming radiation, either in a transmission or backscatter configuration is then analysed. Noting that Raman effect is orders of magnitude less prone to occur when comparing to fluorescence. To circumvent that a good choice of wavelength of the laser source is of major importance to avoid wavelengths that provide too much fluorescence with the sample at question, as it happens when using light in the visible spectrum to analyse biological samples.

Albeit all that, Raman effect provides a label free and quick way to characterize the samples at question. Raman spectroscopy applied to biological tissue is already being pursued at an academical level, with some pursue for commercial applications. The major application, that this dissertation gives focus, is for cancer characterization and discrimination in human tissue. From literature reviewed it is already being applied to digestive tract malignancies along with breast ones. Also noting other applications in other tissues ranging from soft tissues like brain to hard tissues such as bone. Raman spectroscopy is also being applied in conjunction with optical fibres enabling the development of smaller spectroscopy apparatus. Such developments can be used to upgrade current diagnostic techniques in a medical environment.

1.1 Motivation and objectives

This dissertation is being done to a MSc. in Medical Physics, therefore the primary motivation for this work is quite straightforward. To utilize known and well understood physical phenomena together with advancements in optical fibres to improve tracking of diseases as prevention can be seen as more desirable than treatment.

The second motivation point is the fact that Medical Physics is underrepresented in this country, so this work is also done with prospects of bringing more relevance to this profession while also giving precedence for more research in the implementation of optical technologies for disease tracking and prevention.

For last, curiosity brought motivation. The wanting to know more, how physics is applied to medical advancements and wanting to be part of it.

In order to obtain the desired results and establish the groundwork for further work, being that the development of a fibre-based Raman probe that can be integrated with modern endoscopy techniques, the primary objectives of this dissertation are the following:

- Study Raman effect and present state of the art medical implementations.
- Study Raman effect in biological tissues.
- Differentiate between different tissues using Raman spectroscopy.
- Attest viability for usage and improvement in current medical solutions.

1.2 Thesis organization

In Chapter 1, introduction, motivation and objectives are presented to aid the reader understand where the foundations of this dissertation work stand upon. Also, the major contributions stemming from this work are shown as also the key points to take from this chapter.

In Chapter 2, the research groundwork that the dissertation bases itself off is provided. There is a concise introduction to the Raman effect; biomedical implementations of Raman spectroscopy are also disclosed; closing the chapter some key remarks are emphasised.

In Chapter 3, the results are represented together with their analysis and discussion. On the chapter there is also a reasoning for using household cat mammary tissue is written and closing the chapter the key aspects are summed up.

In Chapter 4, the dissertation conclusions were drawn, future work was also envisioned. Such work would have the objective to develop a smaller Raman spectroscopy system using novelty types of micro structured optical fibres.

With that in mind research was done and is present on the Annex chapter. In Appendix A, optical fibres are presented together with implementations for Raman

spectroscopy shown by works that were found to be relevant for this dissertation and as reference for future work.

1.3 Outputs

J. M. R. Jordão, S. Novais, S. F. O. Silva and O. J. R. Frazão, "An overview of fiber-based Raman spectroscopy for cancer detection", *in 4th JEFFA - Jornadas em Engenharia Física, Física, Física Médica e Astronomia 2019*, Porto, Portugal, May 2019

J. M. R. Jordão, S. Novais, S. F. O. Silva and O. J. R. Frazão, “A brief review of fiber optic based Raman spectroscopy for cancer detection”, *in DCE/19 3rd Doctoral Congress in Engineering,* Porto, Portugal, June 2019

Chapter 2 – State of the art: Raman effect, Biomedical applications

2. Raman effect: introduction

2.1 Principles of Raman Effect

Raman effect was first described in detail by Sir Chandrasekhara Venkata Raman in 1928 that disagreed of it being a “feeble fluorescence” but a new type of secondary radiation, an optical effect that could be analogue with X-ray scattering [1], earning him the Nobel prize in Physics in the year of 1930.

Raman scattering is an inelastic interaction [3]. When a sample is irradiated with light two types of collision might occur: either an elastic one or inelastic, no interaction is also possible. If a photon collides with the sample its energy changes causing either a red-shift (loses energy, Stokes shift) or a blue-shift (gains energy, anti-Stokes shift). Stokes shift is more likely to occur due to practically the entire sample population being on the fundamental level, even so both Stokes and anti-Stokes shift have very low intensities, noting that the cross section of the first is orders of magnitude lower than that of fluorescence.

In order to increase this cross-section various methods were devised one of them involves using two laser beams, pump beam and Stokes beam. These two beams interfere and if this interference matches with the resonance frequency of a molecular bond the molecular bond vibration will be greatly enhanced. See Figure 1. This process can generate three different signals [2]: coherent anti-Stokes Raman scattering (CARS), stimulated Raman scattering (SRS) [3] and coherent Stokes Raman scattering (CRS) [3]. All of them have cross-sections orders of magnitude higher than spontaneous Raman scattering.

Spectroscopy methods that apply Raman effect can then perform highly precise, label-free characterisation of samples. This together with the evolution of optical fibres permit the creation of novel, small scale probes that can enhance current *in vivo* endoscopic techniques for cancer detection.

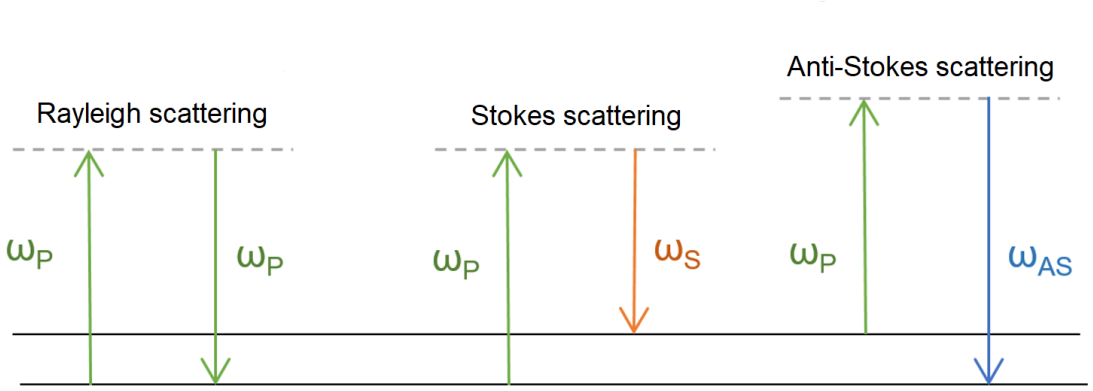

Figure 1. Raman effect diagram, when a scattered photon is red-shifted (less energy) the interaction is named Stokes scattering. If it is blue-shifted an Anti-Stokes scatter has occurred, adapted from [3]

Raman spectroscopy data is typically presented in wavenumbers, unit cm^{-1}. The conversion from cm^{-1} to *nm* is simple and straightforward being it only a unit conversion as shown on the following formula.

$$wavenumber\ (cm^{-1}) = \frac{10^7}{wavelength\ (nm)} \tag{1}$$

And therefore, Raman shifts, Δw, from a known wavelength, λ_1, to a corresponding known second wavelength, λ_2, are calculated as follows:

$$\Delta\omega = \frac{\lambda_1 - \lambda_2}{\lambda_2\lambda_1} \times 10^7 \tag{2}$$

For example, purposes a 785 nm excitation laser with a corresponding 1655 cm^{-1} Raman shift gives a wavelength 902.21 nm for the Raman signal or a 909.09 nm laser with a 1000 nm Raman wavelength corresponds to a 1000 cm^{-1} Raman shift. Pure compounds with well-defined Raman peaks are used as calibration standards in Raman spectroscopy. The system collects the signal from such compounds and its result is compared with known data.

2.2 Applications in biomedical solutions

2.2.1 Mammary tissue

Several works were reviewed that analyse breast tissue with Raman spectroscopy, some of the works are not from human breast tissue and the reason is further explained in Chapter 4. As can be seen checking Table 1 the main ranges of analysis are the 800 – 1800 cm^{-1} (fingerprint zone) and 2800 – 3350 cm^{-1} (dominated by lipids and water) zones.

The Raman signal of these regions is constituted by a myriad of biomolecules, from lipids, proteins, carotenoids, amino acids and nucleic acids mostly. Some mineral material is identified when in the presence of calcifications.

From the reviewed works some bands were deemed more important than others. Such bands include the 1657 cm^{-1} and 1442 cm^{-1} [4, 5] that are argued, trough empirical evidence, as peaks that can be used to distinguish between healthy and lesioned tissue. Other bands would be ones associated with amino acids [6 – 8], proteins [4, 6 – 12], nucleic acids [8, 9, 12], calcifications [13], collagen [4, 7, 12]. As spectra that is dominated by such peaks is deemed as lesioned tissue, either it being a benign tumour or a grade of malign tumour. There are reports of malignant tissue also having presence of interstitial water as shown by the 3311 cm^{-1} peak [6, 10, 14]. Such case might be due to cancer cells being largely composed of proteins that are hydrophilic [15].

In contrast normal tissue is dominated by lipids, has presence of carotenoids [6, 10, 14, 15] and has no calcifications on it. The peaks for carotenoids mentioned are at 1158 cm^{-1}, 1161 cm^{-1}, 1520 cm^{-1}, 1527 cm^{-1} and 1558 cm^{-1}. Another aspect of interest is that normal tissue Raman signal has lesser contribution of fluorescence than that of lesioned tissue, leading to a less intense signal overall. As title of example, Figure 2 illustrates an example of expected Raman spectroscopy signal from normal tissue, malignant tissue and benign tissue, adapted from [13].

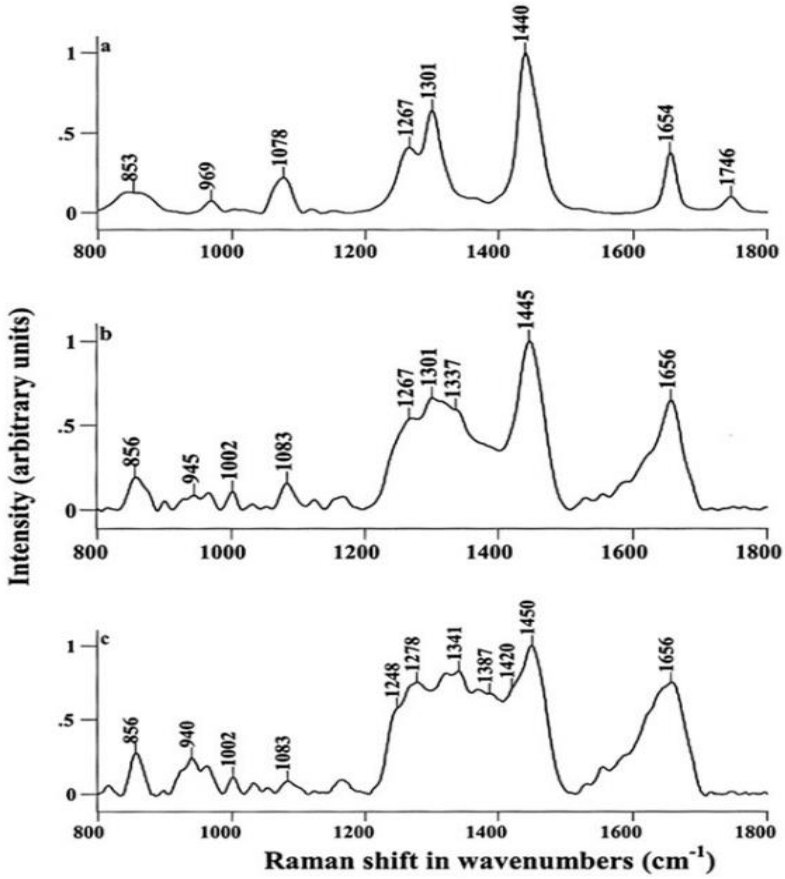

Figure 2. Example of collected spectra from normal breast tissue (a), malignant (b) and benign (c). Adapted from [13].

Table 1 has a roundup of the beforementioned reviewed literature on the topic of Raman spectroscopy in mammary tissue. On the first column is the work reference number, second column has the peaks studied on same work and the third column has all the biomarkers determined on the article. Important bands present would be ones centred near 1440 cm^{-1} and 1660 cm^{-1} for being empirical evidence of tumoral tissue [4]; bands centred near known carotenoids peaks: 1158, 1520, 1527; peaks that are enhanced in malignant tissue [11]: 1545, 1585, 1605 and amino acid peaks such has: 757 cm^{-1}, 829 cm^{-1}, 853 cm^{-1}, 856 cm^{-1}, 936 cm^{-1}, 1002 cm^{-1}, 1004 cm^{-1}, 1026 cm^{-1}, 1045 cm^{-1}, 1153 cm^{-1}, 1156 cm^{-1}, 1182 cm^{-1}, 1208 cm^{-1}, 1515 cm^{-1}, 1549 cm^{-1}, 1585 cm^{-1}, 1610 cm^{-1}

Table 1. Reviewed literature of Raman spectroscopy of mammary tissue

Reference	Important peaks/ bands (cm^{-1})	Markers
[4]	1004, 1262, 1442, 1452, 1657, 1660	Amide I, Amide III, Phenylalanine, Proline, Hydroxyproline, Collagen, Lipids
[6]	1400 – 3000 2800 – 3000 1558 3311	Fatty acids, Proteins, Amino acids, Carotenoids, Water
[7]	728, 757, 782, 829, 853, 1003, 1045, 1096, 1300, 1442, 1460, 1549, 1575, 1656, 1665, 1744 1662 – 1664, 1739 – 1745, 1759 – 1762	Amide I, Tryptophan, Tyrosine, Taurine, Lipids, Ester, Phenylalanine, Proteins, Cholesterol
[8]	856, 936, 1002, 1004, 1026, 1028, 1153, 1156, 1208, 1448, 1515, 1585, 1610, 1662, 800 – 985, 1120 – 1690, 1200 – 1295	Amide I, Amino acids, Lipids, Proteins Nucleic acids, Amide III
[9]	1260, 1442, 1662, 800 – 960, 1080 – 1400, 2700 – 3500	Amide I, Collagen, Lipids, Phospholipids, Proteins, Acyglycerides, Amide II, Amino acids, Acyl chains, Cholesterol, Nucleic acids
[10]	558, 842, 972, 977, 1004, 1098, 1116, 1158, 1240, 1269, 1444, 1518, 1560, 1660, 1740, 1750, 2854, 2888, 2926, 2940, 3009, 3311	Carotenoids, Fatty acids, Lipids, Water, Proteins
[11]	750, 821, 1004, 1080, 1087, 1156, 1172, 1223, 1262, 1306, 1318, 1358, 1378, 1441, 1453, 1460, 1521, 1545, 1550, 1585, 1589, 1605, 1656, 1663, 1746, 2727, 2854, 2935, 1330 – 1380	Amide I, Amide II, Amide III, Lipids, Proteins

[12]	788, 850, 1070, 1098, 1267, 1301,1450, 1660	Collagen, Lipids, Nucleic acids
[13]	1440, 1445, 1450, 1650, 1657, 1746, 600 – 980, 1140 – 1390, 1390 – 1510, 2680 – 3100	Phospholipids, Carotenoids, Acyglycerides, Amide I, Amide II, Amide III
[14]	2800 – 3000 1158, 1161, 1520, 1527, 3311	Water, Lipids, Carotenoids
[15]	1000 – 1600	Carotenoids

2.2.2 Digestive Tract

As can be seen at the Appendix, Raman endoscopic systems were already developed for clinical use. There are several research works that apply Raman endoscopy to *ex vivo* and *in vivo* cancer detection [16-28]. Since endoscopy requires the insertion of a probe it can only be performed in human cavities like the digestive tract.

As per analysis of the works there are key aspects that are worth of noting. The main markers in the Raman signal are peaks of biomolecules and cells (nucleic acids, proteins, lipids, collagen, glycogen, blood and others). Due to this, the range of acquired signals mainly goes from 800 cm^{-1} to 1800 cm^{-1} using near infrared Raman spectroscopy (NIR-RS). But, there are also studies using high wavenumber Raman spectroscopy (HW-RS) for up to 3700 cm^{-1} [19, 23, 25] that collect Raman signal from water content in the tissues, note that the 1800 – 2800 cm^{-1} range provides no relevant information [33]. Classification tools such as linear discriminant analysis (LDA) and principal component analysis (PCA) are often used [16, 18-21, 24, 26, 27]. Also, remarks are made in main suspects that may help in differentiating normal tissue from cancerous tissue from abnormal nuclear activities such as: decrease in lipids presence in malignant ulcerous lesions [16]; bandwidth broadening at 1665 cm^{-1} and red shift around 1445 cm^{-1} for cancer tissue [17]; difference in peak intensity between cancer and normal tissue, with signal (in cm^{-1}) from cancer tissue being higher in the 1070, 1323, 1345, 1576, 1588,

1467, 1618, 1662 and 1685 peaks [20, 26] and lower in the 855, 1019, 1065 and 1745 [20, 26]; an inversion in spectral intensity centred at 1200 cm^{-1} is verified [26] and at 1230 cm^{-1} [18]. An example of Raman signal, from digestive tract, is illustrated in Figure 3.

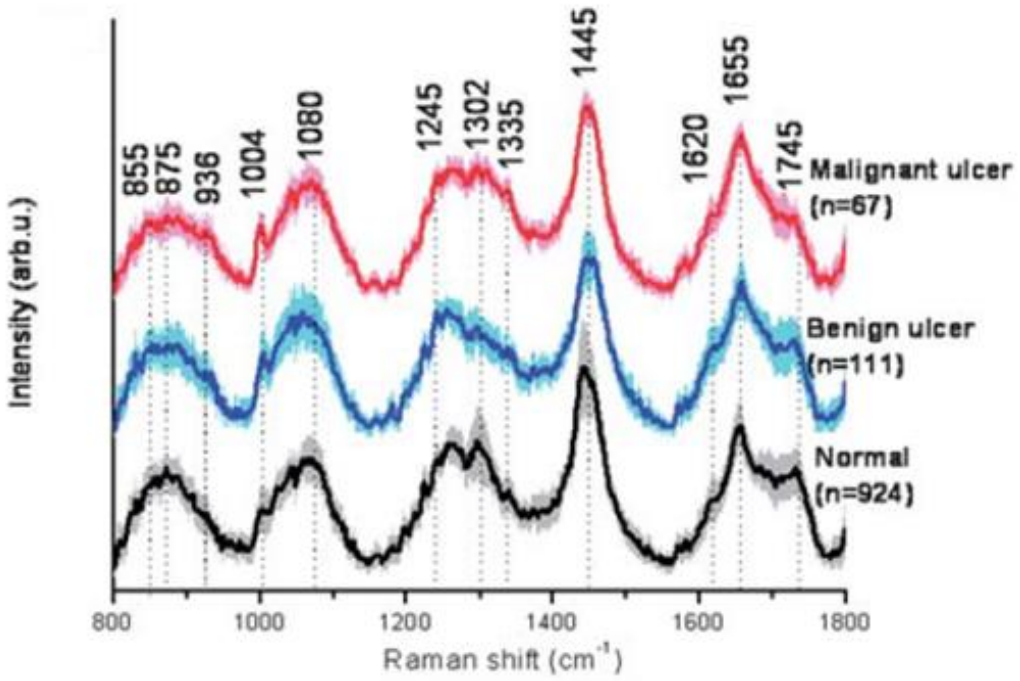

Figure 3. Raman spectra from normal stomach tissue and malignant and benign ulcers, adapted from [16].

In Table 2 a roundup of key aspects from digestive tract reviewed literature is presented. In a similar fashion as Table 1, the first column is the reference number of the article, second column has the location studied in that work, third column has the studied malignancy, the fourth column has the peaks found and for last the fifth column has all the biomolecules that correspond to the found peaks. Raman peaks that might prove of relevance would have to be ones associated with proteins and amino acids (especially if linked to collagen presence), such as: 855 cm^{-1}, 1588 cm^{-1}, 1467 cm^{-1}, 1662 cm^{-1}, 1685 cm^{-1}, and nucleic acids with peaks being: 1323 cm^{-1}, 1345 cm^{-1}. Also, peaks centred near 1440 cm^{-1} and 1660 cm^{-1} with them being empirical evidence of neoplasms [4].

Table 2. Collection of biomedical applications of Raman endoscopy for cancer detection in the digestive tract.

Ref.	Location	Malignancy	Important peaks/ bands (cm^{-1})	Markers
[16]	Stomach	Malignant and ulcerous lesions	800–900 1000–1100 1245–1335 1440–1450 1500–1800	Proteins, DNA, Lipids and Blood
[17]	Stomach	Epithelial neoplasia	1445 and 1655	Nucleic acid, Phospholipids and Histones
[18]	Stomach	Gastric adenomatous polyp Adenocarcinoma	853, 936, 1003, 1032, 1174, 1208, 1323, 1335, 1450, 1640, 1655, 1675	Proteins, Lipids, Carbohydrates and Nucleic acids
[19]	Stomach	Dysplasia Adenocarcinoma	853, 1004, 1078, 1210, 1265, 1302, 1335, 1445, 1618, 1655, 1745, 2850, 2885, 2940, 3250, 3300	Proteins, Nucleic acids, Lipids and Water
[20]	Oesophagus	Oesophageal cancer	875, 936, 1004, 1078, 1265, 1302, 1335, 1445, 1618, 1655, 1745	DNA, Histones, Triolein, Collagen and Glycogen
[21]	Oesophagus	Barret's oesophagus Neoplastic tissue	487, 498, 686, 863, 933, 937, 1128, 1360, 1571	Glycogen, Nucleic acids and Proteins
[22]	Oesophagus	Barret's oesophagus	1004, 1335, 1576, 1655	Phenylalanine, Proteins and DNA
[23]	Cervix	Cervical dysplasia	854, 937, 1001, 1095, 1253, 1313, 1445, 1654, 2946, 3400	Proteins, Lipids, Glycogen, Nucleic Acids and Water
[24]	Colon	Ulcerative colitis	610, 755, 896, 1044,1079,1081,1098, 1102, 1155, 1246, 1256, 1262, 1314, 1331, 1386, 1613	Proteins, Lipids, Nucleic acids, Cholesterol, Phospholipids and Collagen

[25]	Colon	Adenocarcinoma Tubular adenomas Hyperplastic polyps	1003, 1263, 1275, 1318, 1448, 1467, 1582, 1634, 1657, 2850, 2930	Phenylalanine, Amide III, Amide I, Proteins and Lipids
[26]	Colon	Adenocarcinoma	800-1800	Nucleic acids Proteins and Lipids
[28]	Oesophagus	Barret's oesophagus	490, 492, 574, 638, 731, 771, 782, 885, 933, 937, 1018, 1086, 1021, 1095, 1110, 1128, 1334, 1360, 1511, 1621	Glycogen, Nucleic acids and Proteins

2.2.3 Review of other biological samples

Raman spectroscopy is a versatile technique not being limited to only analyse digestive tract and mammary tissues. On this point a brief overview of other tissue applications are presented.

Larsson and Hellgren [29] using 488 nm light studied samples of blood plasma. A result they uncovered was the existence of differences in carotenoid spectral regions between patients with cancer and without. Verma *et al*., [30] would later confirm this finding.

Differences between spectra of calcifications from both coronary artery and aortic valve where studied carried out by Clarke *et al*. [31] using 514.5 nm excitation light. Differences where suggested to stem from different structures and organizations of mineralized deposits. Carotenoids where also identified in atherosclerotic lesions; the 514.5 nm light coincides with the absorption region of carotenoids resulting in more intensity from these modes [32].

Spectra of malignant lesions in the gynaecological tract, namely: ovarian, cervical, uterine and endometrial tissues appear to be similar between them from the work of Alfano *et al*., [33]. Besides peaks due to amide (1650 cm^{-1}, 1445 cm^{-1}, 1240 cm^{-1}, 1260 cm^{-1}) some pathologies showed a peak of tryptophan near 1330 cm^{-1}.

A ratio of grey matter to white matter was developed by Ozaki *et al*., [34] this was done studying spectra from rat brain samples. The bands from proteins and phospholipids were consistent with chemical composition of the samples and as such the ratios of these peaks, lipids and proteins, was used to evaluate the ratio of grey to

white matter. Differences between human brain healthy tissue and brain tumours was analysed by Mizuno *et al*., [35]. A difference was found in glioma grade III that had much prevalent bands in 1130 cm^{-1} and 856 cm^{-1} comparing to normal tissue. These bands are due to an increase in trans lipids and polysaccharides respectively. Also, a tumour of the arachnoidal choroid plexus, central neurocytoma, exhibited a characteristic band at 960 cm^{-1} that indicated the presence of hydroxyapatite.

Bladder tissue was studied by Feld *et al*. [36], the differences between normal and lesioned tissue appear similar to the differences in normal and lesioned tissue of colon tissue, so similar tissue differences as the ones presented in point 2.2.2. The main differences are that there is an increase in the nucleic acid content with an associated decrease in lipid presence, all this in lesioned tissue when comparing to normal tissue.

Manoharan *et al*., [5] analysed a sarcoma of fatty tissues, liposarcoma, using an 830 nm laser. Malignant tissue presented bands associated to carotenoids (1156 cm^{-1} and 1528 cm^{-1}) and the 1442 cm^{-1} and 1666 cm^{-1} bands suffered an alteration due to CH_2 bending modes and C=C stretching.

Chicken bone was compared to synthetic hydroxyapatite and human tooth samples were studied by Nie *et al*., [37]. Chicken bone presented bands due to apatite at 451 cm^{-1}, 960 cm^{-1} and 1072 cm^{-1}. Collagen spectrum, namely bands of proline and hydroxy proline were also present. Tooth also presented apatite peaks when sampling the enamel, closely to 96.5% inorganic material [4], at 591 cm^{-1}, 961 cm^{-1}, and 1071 cm^{-1}. Dentine and root spectra showed that proteins modes are dominant, which is consistent to an increased protein content (an increase of circa 25% [4]).

2.3 Closing Remarks

Raman spectroscopy enables fast, label free discrimination of the molecular components in the sample analysed. Trough analysis of such components a judgement can be done regarding the tissue being sampled.

Of interest is the utility for cancer tracking, as seen in referenced works (see section 2.2), where fast acquisition times are doable with also high precision in discerning between benign and malignant tissues.

In conjunction with the latest optical fibres (see Appendix), *in vivo* Raman spectroscopy sampling of biological tissues is possible. Thus, permitting the addition of a Raman spectroscopy probe to current endoscopy techniques.

With such, the proposal of this dissertation is the analysis of both healthy and lesioned tissue in order to assert the conclusion done through the reviewed work and to try to give more insight regarding the molecular composition of biological tissue, especially malignant one.

To realise such, the most important albeit general aspects taken for the Raman spectroscopy is the laser wavelength used. With that in mind, 785 nm excitation wavelength appears to be a suitable wavelength as seen in the works [16, 20, 22, 27].

The Raman signal collected would be divided into two bands, being the first from 800-1200cm^{-1} and the second from 1200 - 1800 cm^{-1} due to signal inversion around the wavenumber. The possible fingerprint peaks to look for would be (in cm^{-1}): 1004, 1335, 1445, 1618 and 1655 for being recurring peaks across multiple works.

Chapter 3 – Raman spectroscopy in mammary tissue

3.1 Introduction

In this chapter, the results of near infra-red Raman spectroscopy (NIR-RS) utilized to probe samples from a household cat mammary tissue are presented. The structure is as follows, first the results of what is determined as being healthy tissue is presented. Afterwards differing spectra is presented. After all results are shown comparisons between the different spectra is done. At last the concept of “comparative oncology” is further explored. A compilation of the determined results as a takeaway message gives closure to this chapter.

3.2 Instrumentation

The instrument used is an inVia Qontor Renishaw confocal Raman spectrometer. It has 250 mm of focal length, spectral range from 200 – 1064 nm with an efficiency of 30 percent. It is based in lenses directly coupled to a vertical microscope and with a high sensitivity, in the range of 200 – 1064 nm, Peltier cooled, at -70 ºC, CCD with 1024 x 256 pixels. It is also equipped with filters for three excitation lasers: 532 nm, 633 nm and 785 nm with spectral range of 100 – 4000 cm^{-1}. It allows both Stokes and Anti-Stokes Raman spectroscopy with < 10 cm^{-1} starting from the 532 nm laser line. It also possesses three high efficiency diffraction gratings: 1200 lines/mm, 1800 lines/mm and 2400 lines/mm with high spectral resolution < 2 cm^{-1} in all spectral range. The setup photograph and schematic can both be seen in Figure 4.

Figure 4. Experimental setup utilised for present work, in first plane the inVia Qontor Renishaw confocal Raman spectrometer. In the background the set of lasers available: 532 nm, 633 nm and 785 nm.

3.3 Experimental data

All data collected is from cat mammary tissue samples that were provided by the Veterinary Hospital from the University of Évora. It was collected using near infra-red Raman spectroscopy (NIR-RS), at 785 nm, 0.005 mW and a 50x magnification lens. Acquisition times ranged from 1 second to 10 seconds. Many samples were analysed, from which the presented ones in this work were chosen as an example, note that all samples were fixed in formaldehyde. Samples were analysed in multiple far apart regions and differing structures. . Therefore, adding to the acquired spectra some microscope images were also taken (on the scale of a few micrometres to a few millimetres). In the scale of micrometres, the surface appearance is somewhat homogeneous albeit rough. Small darker spots appear, albeit not often, and were sampled along with some dark patches and other elongated structures. All these descriptions can be verified on images presented further along the text. Data is presented in the form of graphs and mappings; mappings are distributions of the of a chosen peak juxtaposed over a white light image of the sample. Peaks chosen are possible fingerprint peaks. For each graph and mapping a brief description and analysis is done comparing the data collected with the referenced literature. Shown spectra are exemplary of the rest of acquired spectra for that sample or for that type of tissue spectra unless said otherwise.

An empirical way of determining between normal and abnormal breast tissue is reported in Manoharan *et al*. [4, 5]. It consists of two points, one being a shift on the 1440 cm^{-1} mode, in normal tissue, towards 1450 cm^{-1} in abnormal one, and the second being a peak broadening and shift from 1650 cm^{-1} to 1667 cm^{-1} also from normal to abnormal tissue. Another aspect is that normal tissue presents much less fluorescence, therefore less intensity, when comparing to abnormal tissue [4, 5].

Another aspect to consider is that spectra from healthy tissue is dominated by lipids, fatty acids and triglycerides [4-15] and that it resembles the spectra from oleic acid [4, 10, 19]. While the spectra from cancerous tissue is mainly dominated by proteins [4, 5, 10, 13] even being compared with pork muscle tissue [10].

Also reported is a higher presence of carotenoids, anti-oxidant agents, in healthy tissue [6, 10, 13, 14, 15], carotenoids appear inside unsaturated fatty acids and triglycerides [10]. Cancerous tissue shows no presence of carotenoids in all works barring Manoharan *et al*., [4, 5] where contradicting results appear in liposarcoma (carotenoids on liposarcoma) [5] versus carcinoma and fibrosis tissues in breast samples

(that present a decrease in carotenoids comparing to healthy breast samples) [4]. A higher presence of collagen in cancerous tissue is also noted, as also certified with histopathology studies [4].

The beforementioned points will be used to help classify the different spectra that will be presented below.

Also note that the names given to tissue and the samples name are not related. From the various samples given only some gave good results and when a letter is used to name a sample it refers to being from the same sample but a different region.

3.3.1 Healthy Tissue

This type of tissue spectra which was attributed as being from healthy tissue was found in all four samples. The determined peaks can be seen in Figure 5. The average was calculated using 29 spectra with 1 second acquisition time each, ~1.63 mW of laser power at 785 nm.

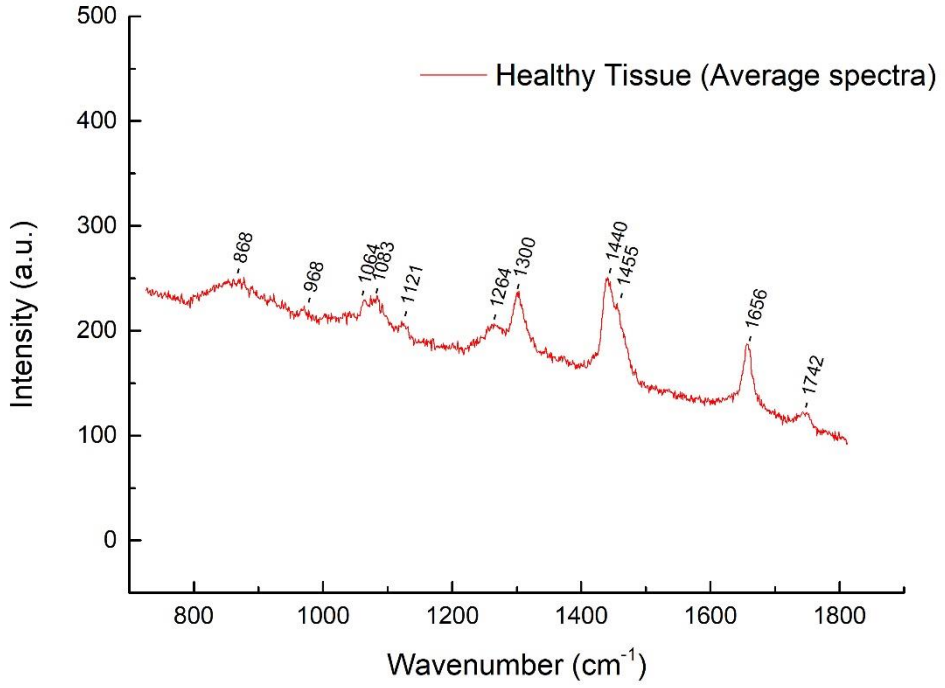

Figure 5. Healthy tissue spectrum obtained through averaging 29 acquisitions.

The origin of the determined peaks present in Figure 5 are as follows:

- 868 cm^{-1} proline.
- 968 cm^{-1} C-C stretching of lipids.
- 1064 cm^{-1} skeletal C-C stretch lipids
- 1083 cm^{-1} C-N stretching mode of proteins (and lipid mode to lesser degree).
- 1121 cm^{-1} C–C stretch (breast lipid).
- 1264 cm^{-1} =C–H in plane bending (lipid).
- 1300 cm^{-1} C-H (CH2) bend, vibrational modes of lipids.
- 1440 cm^{-1} vibrational modes of lipids.
- 1455 cm^{-1} no reference found.
- 1656 cm^{-1} amide I (C=O stretching mode of proteins, a-helix conformation)/C=C lipid stretch.
- 1742 cm^{-1} C=O stretch (lipid), vibrational modes of lipids.

As mentioned before, the empirical findings, the presence of the 1440 cm^{-1} and 1656 cm^{-1} peaks (the maximum recorded difference was by 4 cm^{-1}) raises the flag as this spectrum belonging to healthy tissue. Checking the peaks is easy to notice that all of them can be attributed as being originated from lipids with some, but few, protein contributions in-between which is another pointer towards that belief. Denote that both carotenoids and collagen are absent from these spectra.

Figure 6 presents comparisons between spectra from different samples. Note that these spectra were acquired with a longer acquisition time than the ones shown on Figure 5, namely of 10 seconds, while maintaining the rest of the parameters.

All peaks present in Figure 6 can be seen in Figure 5, albeit the 1083 cm^{-1} and 1455 cm^{-1} peaks are somewhat “hidden” due to present noise. Some key aspects to take would be that the peak centred around 1440 cm^{-1} (lipid peak) is the highest peak present in all spectra. And the 1657 cm^{-1} peak is usually below half of the 1440 cm^{-1} peak.

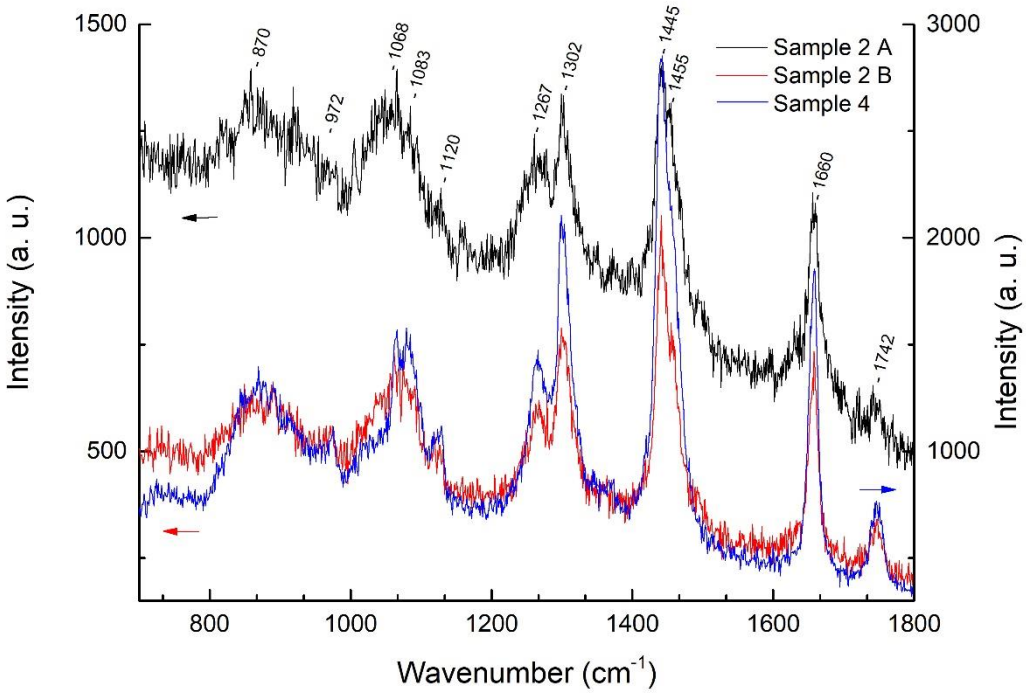

Figure 6. Comparison between two distinct acquirement positions from Sample 2 and spectrum from Sample 4.

Table 3 shows the fraction between proteins (amide I, 1660 cm^{-1}) and lipids (1300 cm^{-1}), it was calculated by doing the fraction between the areas of the corresponding peaks. The idea behind it is that, as said in point 2.2.1, mammary tumoral tissue presents a higher concentration of proteins/amino acids and a degradation of lipids [4 – 12], thus the evaluation of such ratios might help at discerning between tissues.

Table 3. Peak area fractions between proteins and lipids contributions from Sample 2 and Sample 4.

	1660/1120 (Amide I/Glucose)	**1300/1120 (Lipid/Glucose)**	**1660/1300 (Amide I/Lipid)**
Sample 2 A	1.346	1.722	0.677
Sample 2 B	1.475	2.012	0.733
Sample 4	1.549	2.288	0.781

On this table it is shown that the proportion of amide I is less than the lipid amount. Joining this information with the one from the previous paragraph it can be argued that the tissue analysed is healthy tissue. Also by comparing the spectra from Figure 6 and

the ratios of Table 3 it might be safe to assume that albeit from different samples it is the same tissue that is being analysed.

3.3.2 Lesion 1

The following picture, Figure 7, is a microscope image taken with 50x magnification of the “patchy” tissue of Sample 1 that presented spectra dubbed as Lesion 1.

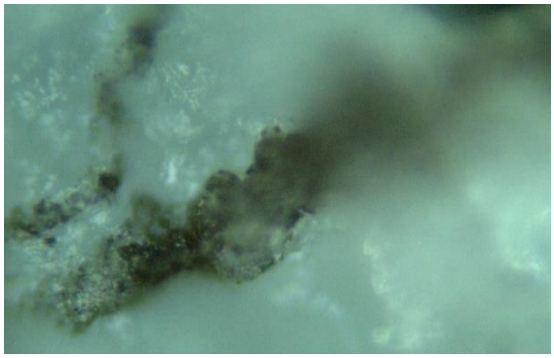

Figure 7. Microscope image taken with 50x magnification of Sample 1 tissue that gave spectra dubbed as Lesion 1.

In Figure 8, the average spectrum shown is made out of spectra only found on Sample 1. The average was calculated using 28 spectra each with 1 second of acquisition time, ~1.63 mW of laser power at 785 nm. The corresponding tissue to this type of spectra was named Lesion 1.

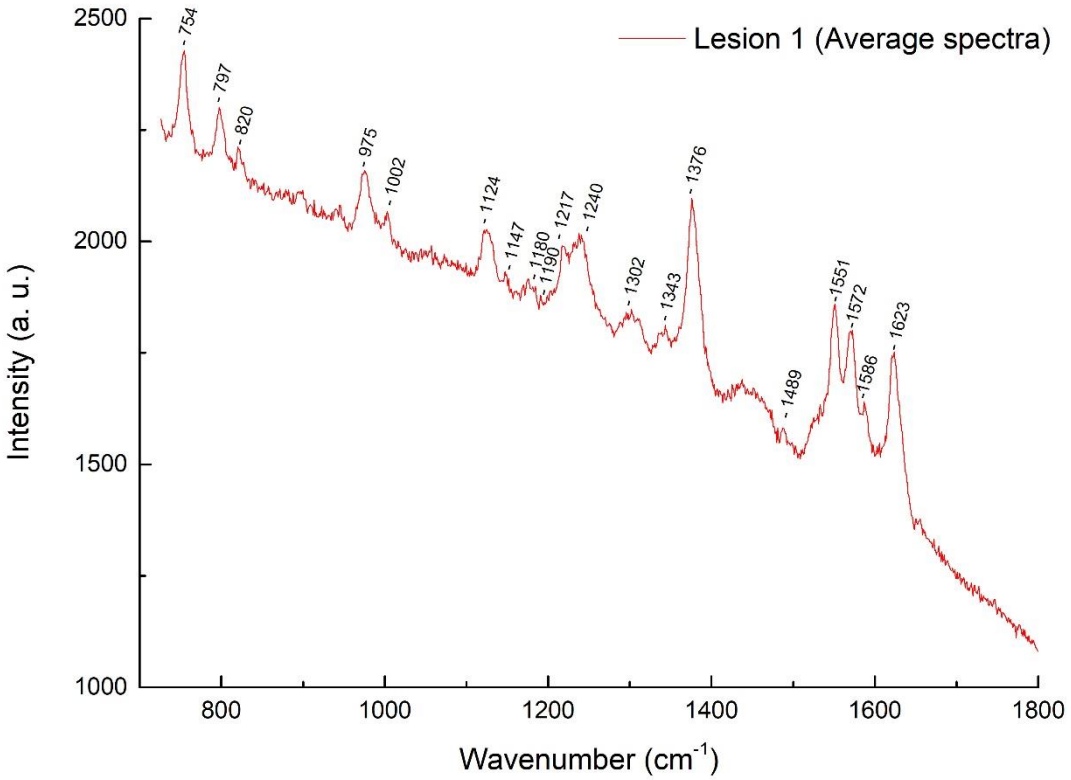

Figure 8. Lesion 1 average spectrum obtained by averaging 28 spectra.

The following are the determined peaks on Figure 8 spectrum:

- 754 cm^{-1} symmetric breathing of tryptophan (amino acid).
- 797 cm^{-1} no reference found.
- 820 cm^{-1} O–P–O stretch (DNA).
- 975 cm^{-1} no reference found.
- 1002 cm^{-1} symmetric ring breathing mode of phenylalanine (amino acid), vibrational modes of proteins.
- 1124 cm^{-1} C–C stretching mode of lipids/protein, C–N stretch, glucose.
- 1147 cm^{-1} no reference found.
- 1180 cm^{-1} cytosine, guanine, adenine (nucleic acids).
- 1190 cm^{-1} $C–C_6H_5$ phenylalanine, tryptophan (amino acids).
- 1217 cm^{-1} amide III: b-sheet.
- 1240 cm^{-1} amide III: collagen (CH_2 wag, C–N stretch)/ pyrimidine bases (C, T).
- 1302 cm^{-1} C-H (CH_2) bend, lipids, CH_2 deformation (lipid)/adenine, cytosine.
- 1343 cm^{-1} CH_3CH_2 wagging mode of collagen.

- 1376 cm^{-1} nucleic acids.
- 1551 cm^{-1} vibrational modes of proteins.
- 1572 cm^{-1} pyrimidine ring (nucleic acids) and haemoprotein.
- 1586 cm^{-1} no reference found.
- 1623 cm^{-1} no reference found.

With these results it can be noticed a rich presence in proteins, followed by nucleic acids and collagen, also there is a lack of glucose bands that were present in the two previous tissues. As mentioned before on section 2.2.1, spectra dominated by proteins [4, 6 – 12], nucleic acids [8, 9, 12] and collagen [4, 7, 12] is deemed as lesioned tissue, it might either be benign or a malign tumour. The high presence of nucleic acids might be explained the same way as having a higher content of proteins present in cancerous tissue. It is likely due to a higher density of cells present on the analysed area.

On Figure 9, three spectra from distinct positions, distinct not only between each other but also from the spectra used on the average in Figure 8, is shown. These spectra where acquired using an acquisition time of 10 seconds, maintaining the other parameters, same as the spectra on Figure 6.

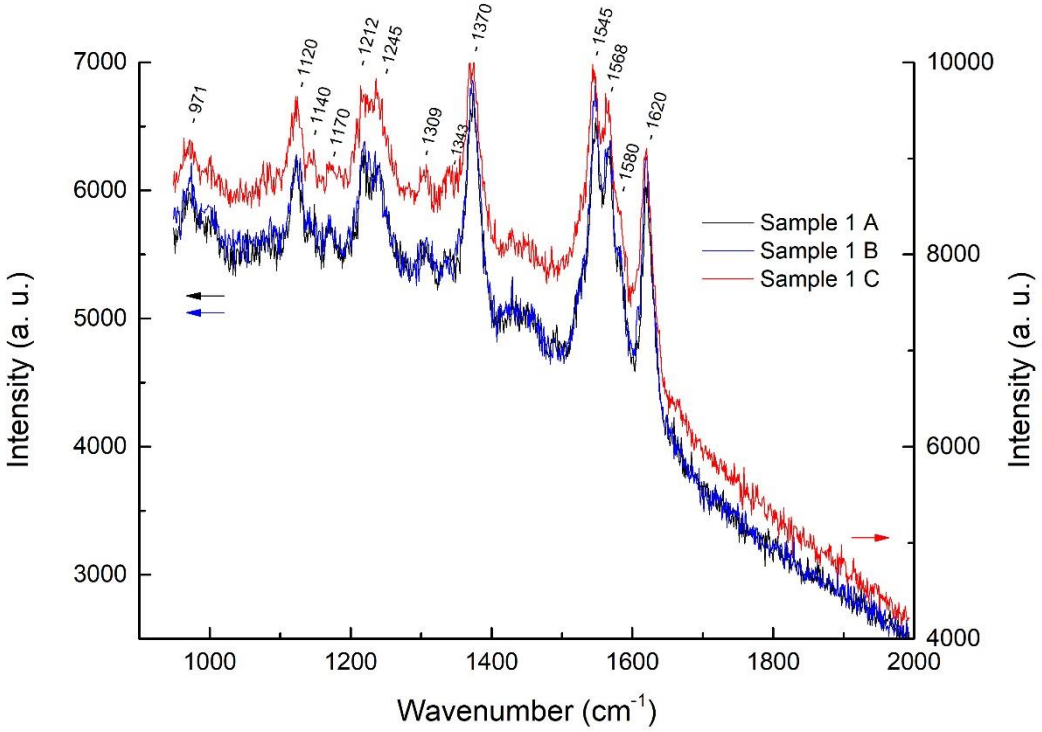

Figure 9. Comparison between spectra acquired in three distinct acquirement positions on Sample 1.

Since the spectra above where not averaged they appear noisier. The highest present peaks (1212 cm^{-1}, 1245 cm^{-1}, 1370 cm^{-1}, 1545 cm^{-1}, 1568 cm^{-1}) are all due to either proteins or nucleic acids with the lipid contributions being only from 1309 cm^{-1}. The 1120 cm^{-1} peak can originate from both proteins, lipids and glucose (a simple sugar). Peaks can still be cross referenced with the above ones albeit the shift.

Table 4 presents the calculated fractions between contributions from proteins (1545 cm^{-1}), lipids (1309 cm^{-1}) and nucleic acids (1374 cm^{-1}). It can be inferred that both proteins and nucleic acids are the dominant species on this type of tissue spectra, both being more intense than glucose and lipids. This further denotes the tissue as having a high presence of cells that are not adipose cells. Which helps to corroborate the idea that the tissue in question, Lesion 1, is not healthy tissue.

Table 4. Peak area fractions between proteins, glycose, and lipids belonging to Sample 1.

	1545/1120 (Proteins/Glucose)	1545/1309 (Proteins/Lipids)	1545/1374 (Proteins/Nucleic acids)
Sample 1 A	1.079	1.617	0.894
Sample 1 B	1.045	1.687	0.814
Sample 1 C	1.064	1.819	0.834

3.3.3 Lesion 2

Depicted in Figure 10 is the average spectra calculated by averaging 23 spectra, each with 1 second of acquisition time, ~1.63 mW of laser power at 785 nm. These spectra were only found in one sample, Sample 3 and named as Lesion 2. The peaks origins are enumerated right after Figure 10.

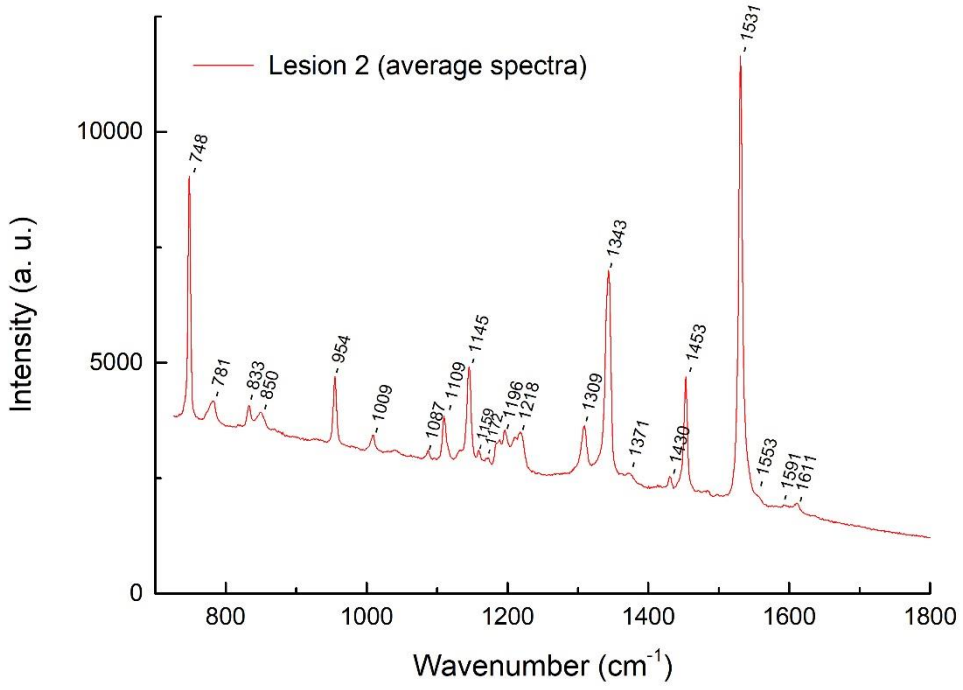

Figure 10. Lesion 2 spectra obtained from averaging 23 spectra.

The peaks origins were determined as to be:

- 748 cm^{-1} no reference found.
- 781 cm^{-1} cytosine, uracil ring breathing (nucleotide).
- 833 cm^{-1} out of plane ring breathing tyrosine (amino acid), O–P–O stretch DNA.
- 850 cm^{-1} ring breathing mode of tyrosine and C–C stretch of proline (amino acid) ring.
- 954 cm^{-1} hydroxyapatite a type II calcification, carotenoid, cholesterol.
- 1009 cm^{-1} phenylalanine, CH_3 rocking coupled with C-C stretching of carotenoids.
- 1087 cm^{-1} C–C stretch, O–P–O– stretch.
- 1109 cm^{-1} no reference found.
- 1145 cm^{-1} no reference found.
- 1196 cm^{-1} no reference found.
- 1218 cm^{-1} amide III: b-sheet.
- 1309 cm^{-1} CH_2 deformation (lipid), adenine, cytosine.
- 1343 cm^{-1} CH_3CH_2 wagging mode of collagen.
- 1371 cm^{-1} guanine, TRP (protein), porphyrins, lipids.
- 1430 cm^{-1} CH_2 deformation (lipid).
- 1453 cm^{-1} CH_2 bending mode of proteins, CH_2(overlapping asymmetric CH_3 bending & CH_2 scissoring (is associated with elastin, collagen and phospholipids).
- 1531 cm^{-1} vibrational modes of proteins.
- 1553 cm^{-1} vibrational modes of proteins.
- 1591 cm^{-1} no reference found.
- 1611 cm^{-1} C=C stretching mode of tyrosine and tryptophan.

This spectra presents various peak contributions from proteins, amino acids, nucleic acids and collagen same as the spectra from Lesion 1, presented before. Differences between them come in lesser presence of lipids and a presence of hydroxyapatite, a mineral form of calcium phosphate with an apatite structure, which is determined as being a type II calcification [13]. Type II calcifications are the more frequent ones and albeit not always they are the result of malignancy [38]. There are also peaks centred at 1309 cm^{-1} and 1453 cm^{-1}, with the latter being a possible shift of the 1440 cm^{-1} peak which was referenced before, section 2.2.1 and section 3.3, as an empirical evidence of a neoplasm [4].

Depicted in Figure 11 are three spectra chosen from many as an example, they were all acquired in different locations from each other, different from the locations of spectra used on Figure 10, and all with an acquisition time of 10 seconds, keeping the rest of parameters. The left-most peak on Figure 11, namely 950 cm^{-1}, is confirmation of presence of type II calcifications.

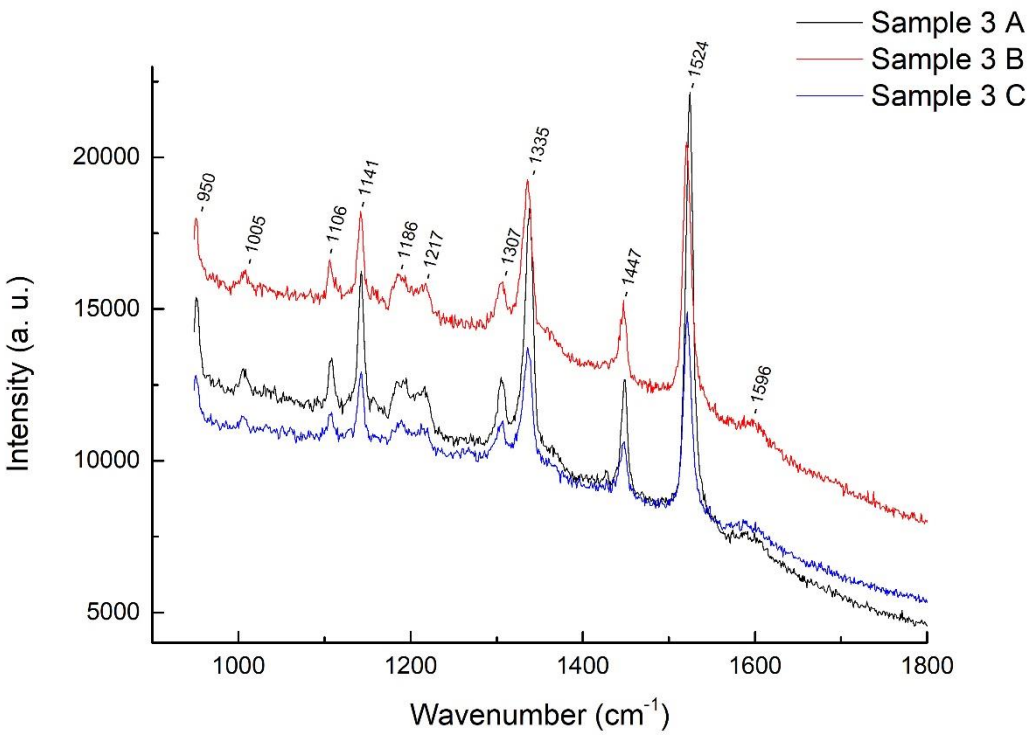

Figure 11. Comparison between three distinct acquirement positions on Sample 3, all with the Lesion 2 spectra.

In Table 5, the ratios between lipids (1448 cm^{-1}), collagen (1335 cm^{-1}), proteins (1524 cm^{-1}) and calcification (950 cm^{-1}) contributions are represented. Their data was calculated from the spectra shown is Figure 11. It can be inferred that proteins (1524 cm^{-1}) are the main contributor followed right after by collagen (1335 cm^{-1}) then lipids

(1448 cm^{-1}). With such major contribution from proteins [4, 6 – 12], collagen [4, 7, 12] with also the presence of a type II calcification [13, 38] it cements the idea that this tissue, Lesion 2, is malignant in nature.

Table 5. Peak area fractions from peaks belonging to Sample 3.

	1448/1524 (Lipid/Protein)	**1335/1448 (Collagen/Lipid)**	**1335/1524 (Collagen/Protein)**	**950/1335 (Calcification/Collagen)**
Sample 3 A	0.438	1.620	0.709	0.439
Sample 3 B	0.459	1.502	0.689	0.436
Sample 3 C	0.457	1.494	0.683	0.433

3.3.4 Lesion 3

In Figure 12, a microscope image that was taken with 50x magnification is presented. Multiple samples presented this type of spectra and this image serves as an example on what the tissue that has this type of spectra may look like. The morphology of the tissue ranged from a filiform appearance to a scar-like one as can be seen on Figure 12.

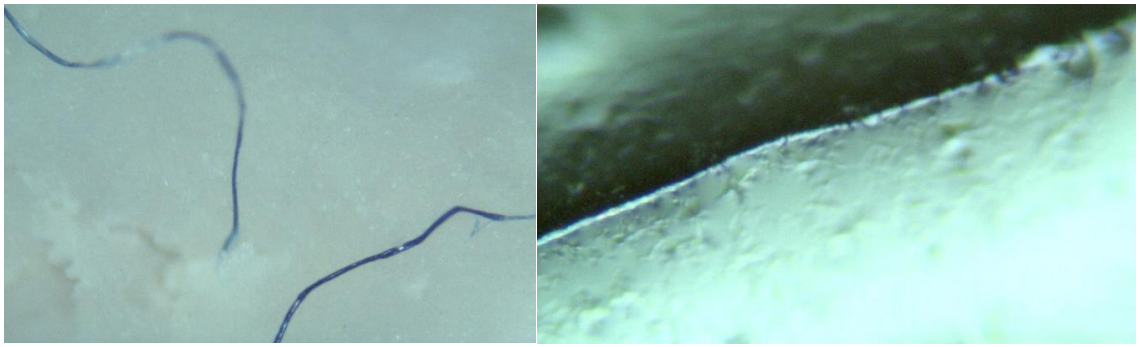

Figure 12. Microscope images of the “filiform appearance” structure, 10x magnification, and the “scar-like” one, with 50x magnification.

On Figure 13, an average spectra is shown. This spectra was done by averaging 38 spectra, where each was acquired in different locations from multiple samples and with 1 second of acquisition time, ~1.63 mW laser power at 785 nm. This type of spectra was named Lesion 3, one peculiarity of it is a doublet appearing at 1575 cm^{-1} – 1585 cm^{-1}.

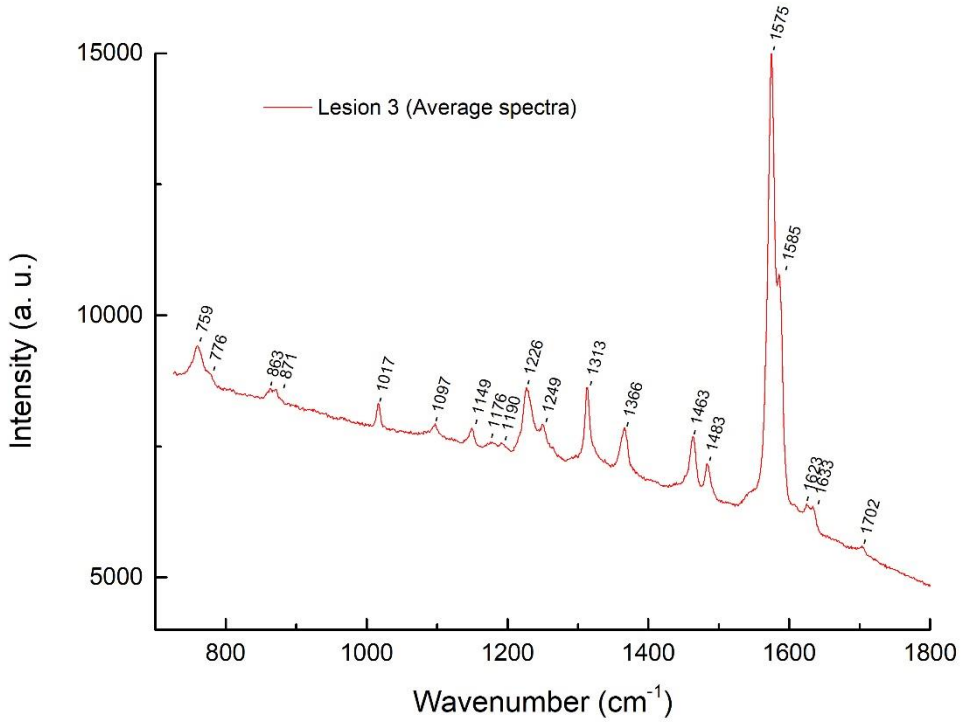

Figure 13. Lesion 3 spectra, average of 38 spectra acquired from different positions across multiple samples.

The sampled peaks, taken from the average spectra in Figure 13, are as follows:

- 759 cm^{-1} tryptophan.
- 776 cm^{-1} C–C stretch of proline, hydroxyproline and tyrosine and v_2 PO_2 stretch of nucleic acids bands).
- 863 cm^{-1} tyrosine, collagen.
- 871 cm^{-1} proline.
- 1017 cm^{-1} no reference found.
- 1097 cm^{-1} O-P-O (stretching PO_2 symmetric (Phosphate II)) of phosphodiesters.
- 1149 cm^{-1} no reference found.
- 1176 cm^{-1} C–H in-plane bending mode of tyrosine.
- 1190 cm^{-1} $C–C_6H_5$ phenylalanine, tryptophan.
- 1226 cm^{-1} Amide III: b-sheet.
- 1249 cm^{-1} Amide III: collagen (CH2 wag, C–N stretch)/ pyrimidine bases (C, T).

- 1313 cm^{-1} CH_3CH_2 twisting mode of collagen, lipids.
- 1366 cm^{-1} guanine, TRP (protein), porphyrins, lipids.
- 1463 cm^{-1} no reference found.
- 1483 cm^{-1} nucleic acid purine bases (guanine and adenine).
- 1575 cm^{-1} pyrimidine ring (nucleic acids) and heme protein.
- 1585 cm^{-1} no reference found.
- 1623 cm^{-1} no reference found.
- 1633 cm^{-1} C-O asymmetric stretching. Calcium oxalate dihydrate, type I calcification.
- 1702 cm^{-1} no reference found.

The results show a high presence of amino acids, proteins, collagen, nucleic acids, a calcification and of interest there is no peak that is purely associated with lipids. Other key notes that are extracted from this type of spectra is the following: as mentioned, there is a well-defined narrow band on the 1575 cm^{-1} – 1585 cm^{-1} range with two distinct peaks present, a doublet. There is a lack of the peak from glucose, that was present in healthy tissue and Lesion 1. The 1300 cm^{-1} and 1440 cm^{-1} peaks that were seen on previous shown spectra, healthy tissue, appear to be shifted to 1313 cm^{-1} and 1460 cm^{-1} respectively and the latter might be empirical evidence of a neoplasm, as stated before. They are the only spectra with a peak centred at 1633 cm^{-1}, which is a type I calcification. This type of calcifications are uncommon when compared to type II and are associated with benign processes [38].

In Figure 14 a comparison between spectra acquired from three different acquisition locations, between two samples, is presented as an example, all were acquired with 10 seconds of acquisition time, keeping the same parameters of power and laser frequency.

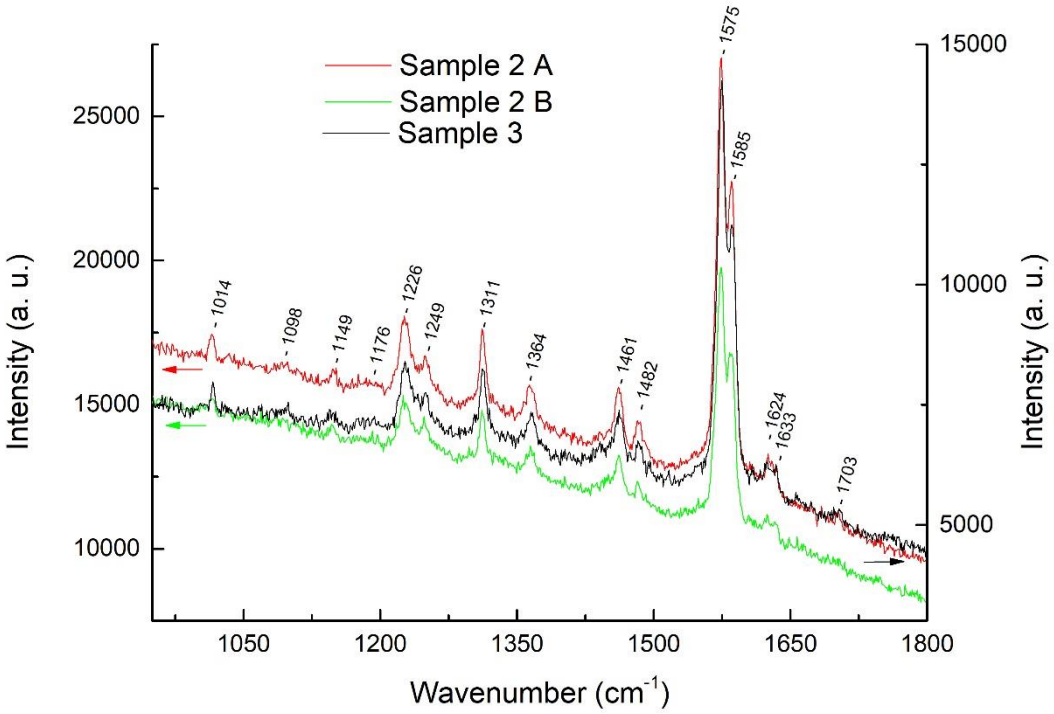

Figure 14. Comparison between Lesion 3 spectra, two originating from Sample 2 and one from Sample 3.

Table 6 presents fractions between the doublet (1585 cm^{-1}/1575 cm^{-1}) and type I calcification (1633 cm^{-1}) with nucleic acids (1482 cm^{-1}), their data was acquired from the spectra presented on Figure 14. From the fact the doublet ratio is quite similar between different spectra it is likely that both peaks have the same species origin and might prove useful for further study.

Due to having a type I calcification [38], high contributions from proteins [4, 6 – 12] and presence of collagen [4, 7, 12] is safe to assume that Lesion 3 spectra is likely to represent a benign neoplasm.

Table 6. Peak area fractions between the doublet, type I calcification and nucleic acids from spectra presented in Figure 14.

	1585/1575 (-/Nucleic acids)	**1633/1482 (Calcification/Nucleic acids)**
Sample 2 A	0.58141	0.486328
Sample 2 B	0.632379	0.436333
Sample 3	0.632834	0.435595

3.4 Comparisons between tissues

Figure 15 presents a comparison between all four different spectra acquired across all samples. All spectra used to average were acquired with same conditions of laser power, ~1.63 mW, and acquisition time, 10 seconds.

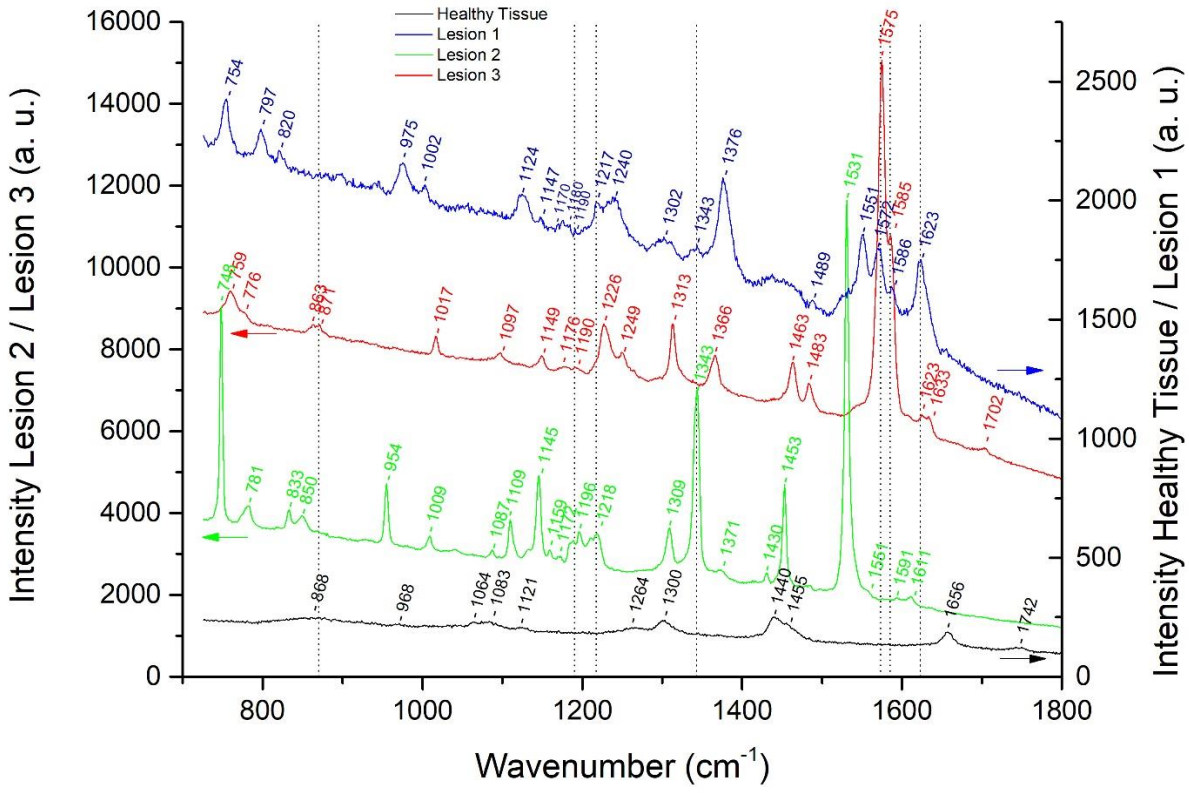

Figure 15. Comparison between the average spectra of all three Lesions and Healthy Tissue.

The first thing of note is as referenced before, healthy tissue has overall less fluorescence than tissue with lesions [4, 13]. Another way to differentiate healthy tissue spectra is that it presents well defined peaks centred at 1440 cm^{-1}, 1656 cm^{-1} and 1742 cm^{-1}.

Lesion 1 tissue spectra are the only ones with four well defined peaks in the 1550 cm^{-1} – 1623 cm^{-1} region, and the 1551 cm^{-1}, 1572 cm^{-1}, 1586 cm^{-1} and 1623 cm^{-1} peaks. Also presents the 1376 cm^{-1} peak. And while Lesion 3 also presents the 1572 cm^{-1},1586 cm^{-1} (at 1575 cm^{-1} and 1585 cm^{-1} respectively) and 1623 cm^{-1} they are not near as intense. The only spectra not having a peak in the 1440 cm^{-1} – 1460 cm^{-1} range.

Lesion 2 tissue spectra are the ones with three very narrow peaks in 748 cm^{-1}, 1343 cm^{-1} and 1531 cm^{-1}. It is also the only one with a type I calcification peak (954 cm^{-1}). Albeit Lesion 1 does also present the 1343 cm^{-1} peak it is not as narrow nor intense comparatively. As mentioned before Lesion 1 has a possible shift of the 1440 cm^{-1} peak towards 1453 cm^{-1} [4].

Lesion 3 spectra presents narrow bands at 1575 cm^{-1} and 1585 cm^{-1} while also having a type I calcification present (in 1633 cm^{-1}). The 1463 cm^{-1} peak is a possible shift of the 1440 cm^{-1} peak as previously written [4].

There appears also to be a shift of the 1300 cm^{-1} peak towards 1309 cm^{-1} in Lesion 2 and 1313 cm^{-1} in Lesion 3 that was not previously mentioned in the reviewed literature. And since both were tentatively classified as being a malign neoplasm and a benign one, respectively, this result might also be a major empirical evidence in helping to differentiate between neoplasms to add to previously mentioned before by Manoharan *et al.* [4].

There are several other peaks that can be observed on Figure 15 that are not discussed, namely: 748 cm^{-1} (Lesion 2), 797 cm^{-1} (Lesion 1), 975 cm^{-1} (Lesion 1), 1017 cm^{-1} (Lesion 3), 1109 cm^{-1} (Lesion 2), 1175/1176 cm^{-1} (Lesions 1 and 3), 1196 cm^{-1} (Lesion 2), 1226 cm^{-1} (Lesion 3), 1249 cm^{-1} (Lesion 3), 1463 cm^{-1} (Lesion 3), 1585/1586 cm^{-1} (Lesions 1 and 3), 1591 cm^{-1} (Lesion 2), 1623 cm^{-1} (Lesions 1 and 3) and 1702 cm^{-1} (Lesion 3). The explanation is that no literature was found to determine the origin of those peaks.

On Figure 16, are depicted two mappings that provide the peak intensity distribution comparing between healthy tissue and Lesion 3 tissue, From the same sample. Albeit the peaks compared appear close, it proves enough to trace zones that

closely approach the tissue morphology. Mappings are distributions of the of a chosen peak juxtaposed over a white light image of the sample.

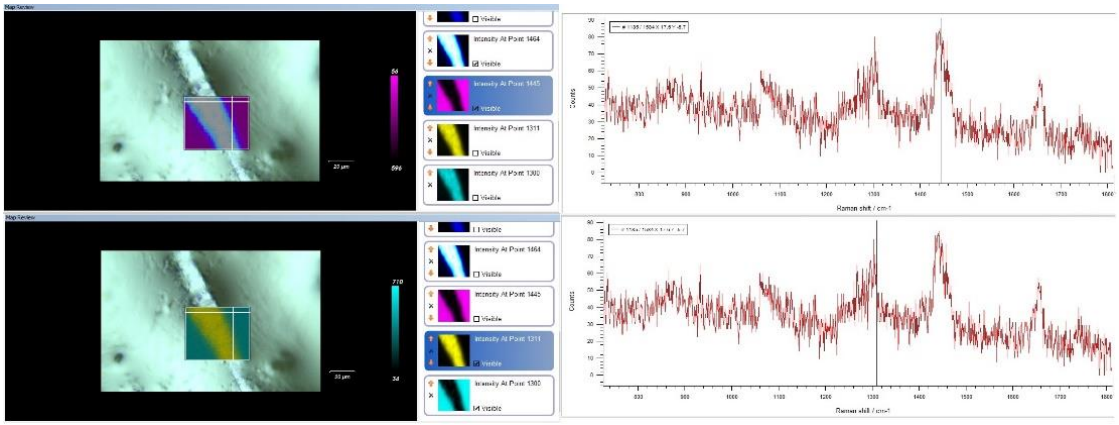

Figure 16. Two mappings, as example, with the over position of peaks from healthy tissue and Lesion 3 tissue. The over posed peak intensity distribution is respectively the 1445 cm^{-1} – 1464 cm^{-1} (top left) and 1300 cm^{-1} – 1311 cm^{-1} (bottom left) peaks. Right side is the spectra acquired on the point marked by the crosshair of the left side.

At Table 6 the roundup of peaks that were found in the studied tissues and with known origins is presented along with the determined sources of each peak.

Table 6. Compilation of peaks found in the sample's analysis.

Peak (cm^{-1})	Origin	Sample
754	symmetric breathing of tryptophan	Lesion 1
759	Tryptophan	Lesion 3
776	C–C (C–C stretch of proline, hydroxyproline and tyrosine and stretch of nucleic acids bands	Lesion 3
781	cytosine, uracil ring breathing (nucleotide)	Lesion 2
820	O–P–O stretch	Lesion 1
833	out of plane ring breathing tyrosine (amino acid), O–P–O stretch DNA	Lesion 2
850	ring breathing mode of tyrosine and C–C stretch of proline (amino acid) ring	Lesion 2
863	tyrosine, collagen	Lesion 3

868 – 871	Proline	Healthy Tissue Lesion 3
954	Hydroxyapatite (type II calcification), carotenoid, cholesterol	Lesion 2
968	C-C stretching of lipids	Healthy Tissue
1002	symmetric ring breathing mode of phenylalanine (amino acid), vibrational modes of proteins.	Lesion 1
1009	phenylalanine, CH_3 rocking coupled with C-C stretching of carotenoids	Lesion 2
1064	Skeletal C–C stretch lipids	Healthy Tissue
1083	C–N stretching mode of proteins (and lipid mode to lesser degree)	Healthy Tissue
1087	C–C stretch, O–P–O– stretch	Lesion 2
1097	O-P-O (stretching PO_2 symmetric (Phosphate II) of phosphodiesters	Lesion 3
1121	C–C stretch (breast lipid)	Healthy Tissue
1124	C–C stretching mode of lipids/protein, C–N stretch, glucose	Lesion 1
1170	C–H in-plane bending mode of tyrosine	Lesion 1
1180	cytosine, guanine, adenine	Lesion 1
1190	$C–C_6H_5$ phenylalanine, tryptophan	Lesion 1 Lesion 3
1217 - 1218	amide III: b-sheet	Lesion 1 Lesion 2
1240	amide III: collagen (CH_2 wag, C–N stretch)/ pyrimidine bases (C, T)	Lesion 1

1264	=C–H in plane bending (lipid)	Healthy Tissue
1300	C-H (CH2) bend, vibrational modes of lipids	Healthy Tissue
1302	C-H (CH_2) bend, lipids, CH_2 deformation (lipid)/adenine, cytosine	Lesion 1
1309	CH_2 deformation (lipid), adenine, cytosine	Lesion 2
1313	CH_3CH_2 twisting mode of collagen, lipids	Lesion 3
1343	CH_3CH_2 wagging mode of collagen	Lesion 1 Lesion 2
1366	guanine, TRP (protein), porphyrins, lipids	Lesion 3
1371	guanine, TRP (protein), porphyrins, lipids	Lesion 2
1376	nucleic acids	Lesion 1
1430	CH_2 deformation (lipid)	Lesion 2
1440	Vibrational modes of lipids	Healthy Tissue
1453/1455	CH_2 bending mode of proteins, CH_2(overlapping asymmetric CH_3 bending & CH_2 scissoring (is associated with elastin, collagen and phospholipids)	Lesion 2 Healthy Tissue
1483	nucleic acid purine bases (guanine and adenine)	Lesion 3
1531	vibrational modes of proteins	Lesion 2
1551	vibrational modes of proteins	Lesion 1
1572-1575	pyrimidine ring (nucleic acids) and haemoprotein	Lesion 1 Lesion 3
1611	C=C stretching mode of tyrosine and tryptophan	Lesion 2

1633	C-O asymmetric stretching. Calcium oxalate dihydrate, type I calcification	Lesion 3
1656	Amide I (C=O stretching mode of proteins, a-helix conformation)/C=C lipid stretch	Healthy Tissue
1742	C=O stretch (lipid), vibrational modes of lipids	Healthy Tissue

3.5 Comparative oncology

As said before, some similarities between cancerous tumours found in humans and those found in animals led to the concept of “comparative oncology”, thus permitting a cross evolution of cancer research [14]. Comparative oncology studies cancer pathogenesis and new treatment options for occurring cancers in animals. Majority of focus is put on the domestic dog but more species like cat, horse and ferret are of interest [39]. It has the advantage of bringing more data to cancer research since natural occurring cancers in animals can be translated to humans. If the animal in study presents a good or representative model of cancer evolution that simulates human pathological conditions, then that animal is a good candidate to study [40]. With that, pet animal cancers are comparable both in size and evolution with human cancers [41]. Another advantage of using animals, especially companion animals such as dogs or cats, is that they cohabit with humans. Sharing the living environment and as likely exposed to carcinogenesis as humans [41], one disadvantage in using such animals so far is the lack of specific tools that are already deployed to human research [41]. Mammary tumour incidence is around 34.5% in cats [42], thus, the focus of this work on the domestic cat, since it is easier to get access to samples and results still hold human clinical interest.

3.6 Conclusion

The results obtained where mostly in check with the reviewed literature. All spectra showed presence of biomolecules with enough difference between tissues to draw a line that differentiates them. In other words it means that healthy tissue showed a prevalence of lipids and lower fluorescence contrasting with the dubbed lesioned tissue. On the other side, lesioned tissue presented more protein content, increase in collagen, more nucleic acids contributions, amino acids, an increased presence of collagen (with presence of proline and hydroxy proline in some spectra). Both types of calcifications (calcium oxalate dihydrate and hydroxyapatite) appear in two distinct

tissues. Of note is that, differing from the literature, carotenoids where not prevalent, actually it was not even found in what was determined as healthy tissue and was a minor presence in one of the lesioned tissues. One explanation might be due to how the samples were preserved as they were fixed in formaldehyde.

Chapter 4 – Conclusion and future work

4.1 Conclusion and future work

In conclusion, the work done was a good step to give insight in Raman spectroscopy techniques and also data analysis methods. Not only that, the results in general were in line with the overviewed literature while also providing more information when talking about specific regions of the spectrum.

Out of the four samples, four types of differing tissue spectra were studied. Tissue determined as being healthy tissue provided spectra dominated by lipids while also having less fluorescence than other tissues spectra. Tissue dubbed as Lesion 1 presented a major presence of proteins, nucleic acids and collagen. Such contributions point to this tissue having a neoplastic nature while not confirming if either a benign or malign neoplasm. Lesion 2 samples showed a high presence of proteins, amino acids, nucleic acids and collagen. Similar to Lesion 1 in that regard. The major differing factor from all other tissues is the presence of hydroxyapatite, a type II calcification. This type of calcifications is more frequent than type I and while not always they are mostly the result of malignancy, making then Lesion 2 a malignant lesion. For last, Lesion 3 has a major contribution from amino acids associated with collagen and has a presence of calcium oxalate dihydrate, a type I calcification. As mentioned before, these are less frequent than type II and are associated with benign processes.

In sum, differing from lesioned tissue, healthy tissue presented a higher contribution from lipids to the spectra while also having a lower baseline of fluorescence. Lesioned tissue showed a major contribution from proteins, increase in collagen content (with proline and hydroxy proline also present) and two types of calcifications, type I (calcium oxalate) and type II (hydroxyapatite), which were found in two differing groups of spectra. Carotenoids, departing from the reviewed literature, were not prevalent. By that, carotenoids were not even found in the determined healthy tissue and one of the lesioned tissues had a minor presence. The way the samples were preserved, fixed in formaldehyde, might explain this case.

The increase in information regarding specific regions of the spectrum might be due to the equipment used and not on the technique itself. Some of this information, if reproduced and validated can increase the accuracy of future Raman spectroscopy discrimination regarding tumorous tissue.

It also opens the path for future work, based on the ground work already done, pursuing to fully develop an *in vivo* Raman spectroscopy endoscope. A possible roadmap can be as follows:

- Use the knowledge gained through this work and devise a miniaturized/portable system.
- Develop a filter tip to apply into optical fibres.
- Incorporate this fibre onto a spectrometer and analyse reference materials and improve the system.
- Step up into fixed breast samples.
- Afterwards into fresh samples.
- Validate the incorporation of such a system into an endoscope in a medical environment.

Appendix A - Brief review of endoscopy based on optical fibres

A.1 Endoscopy using solid core fibres

In the 1990's there was still studies of optical fibre properties being performed as seen in [43] where an analysis of background fibre emission for a typical silica fibre, a forward-scattering fibre geometry study and the determination of the dependence of sensitivity on the type of optical termination and separation is performed. Relevance to this dissertation is present due to fibre background noise analysis and throughput dependence.

Most reports of standard silica optical fibre usage for Raman spectroscopy date back from 1995-2000 [43-49], there was afterwards a shift for other optical fibres. Many of the reported works use a kind of fibre bundle geometry where there is a central fibre for delivery of laser signal and multiple fibres for collection of Raman signal surrounding it.

With Berger *et al*., [44], a 50 µm core diameter wide fibre was used for laser delivery and a 100 µm diameter for collection of signals. A tuneable diode laser emitting at 830 nm with 200 mW optical power was the source. The laser was then holographically bandpass-filtered and coupled into a 50 µm core diameter optical fibre. The fibre guided light onto a dichroic beam splitter apparatus that imaged the excitation fibre's output 1:1 onto the samples. The Raman signal emerging from the sample surface 1:1 imaged onto a collection fibre with a core diameter of 100 µm and numerical aperture of 0.29. The collected signal passed through a holographic notch filter which had an optical attenuation of four at the excitation wavelength and a transmission of 80% of the scattered Raman light. Then, was coupled to a single-stage f/1.8 spectrograph (Holospec, Kaiser Optical Systems) equipped with a transmissive holographic grating and a back-thinned, 512x512 element, LN_2 cooled charge coupled device, CCD, (Tektronix, Princeton Instruments). Spectra from dissolved gases in PBS was gathered and their concentrations were measured using Raman spectroscopy. The schematic is presented in Figure 17.

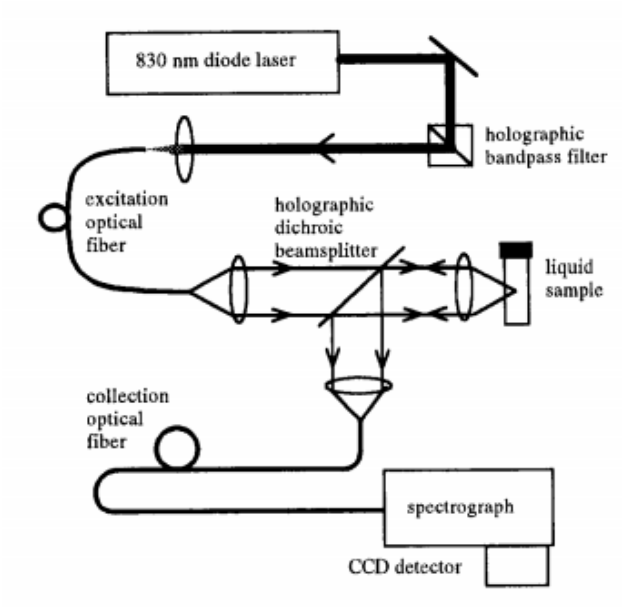

Figure 17. Schematic of the Raman spectroscope. Adapted from [44].

Following up, part of the group [45] employed a 6x1 fibre bundle geometry with all fibres being 100µm wide. Laser source and spectrograph system were the same as in [44]. This time glucose, lactic acid and creatinine concentrations in a phosphate-buffered saline solution were measured.

Raman endoscopic systems built for clinical environment were also pursued, as seen in Brennan *et al*., [46], where two systems were built, namely a “Laboratory system” and a “Clinical system”. The first used an Argon laser pumped Ti:Sapphire system (Coherent Innova 90/Spectra Physics 3900S) outputting close to 350 mW of optical power at 830 nm. No optical fibres were utilized on this system. The “Laboratory system” used a diode laser (SDL 8630) also emitting at 830 nm. Light was both delivered and collected via a “5 French” (~1.7 mm diameter) 3 m long optical probe that was arranged in a 6x1 optical fibre bundle geometry (Fiberguide Ahnydroguide G). All fibres had 200 µm of diameter and were coupled to a *f*/1.8 (Holospec, Kaiser) spectrometer. In the same time period Mahadevan-Jansen *et al*. [47], built a probe using a multimode silica fibre with 200 µm core diameter for the delivery fibre and 100 µm wide collection fibres. A diode laser outputting 15 mW of optical power at 789 nm was utilized. Spot size at analyte surface was 900 µm. One of the fibres guided a 632.8 nm He-Ne laser to help guiding the probe. The objective was to develop a compact fibre optic probe to measure near infrared Raman spectra of human cervical tissue *in vivo* for the clinical diagnosis of cervical precancer.

Various works from Shim *et al*. [48-50] also developed an optical fibre Raman endoscope. In [48] the probe used a 6x1 optical fibre bundle geometry, the diameters for core, cladding and the buffer were 200 µm, 240 µm and 270 µm, respectively (Polymicro Tehcnologies, Phoenix, AZ, USA). A diode laser (SDL, San Jose, CA, USA) was utilized in the 778 ± 10nm band. For spectrographic system a *f*/1.8 (Holospec, Kaiser Optical Systems) was also used. The same system was updated in [49] where a 7x1 bundle of low-OH fibres was used. The width of the fibres were 400 µm and 300 µm for the delivery and collection fibres, respectively, and the probe length was 1.5m. Filters where introduced at 0.0025m from the tip, a bandpass for the delivery fibre and long-pass filters for collection fibres, hereby the system was named IFP (Internally filtered probe) (Figure 18). Laser source and spectrographic system were the same as in [9]. The following year [50] uses the described system together with a 785 nm, ~100 mW incident power, diode laser (Model 8630, SDL, San Jose, CA) to test viability in gastrointestinal endoscopy.

Motz *et al*. [51], also used a probe that can be seen as an IFP (Figure 18, left side). Fibres with 200 µm in core diameter and a 15x1 bundle geometry were used. Both filters and a sapphire ball lens where attached to the bundle tip. The built probe was 4 m long and 3 mm in tip diameter. A diode laser (Process Instruments, Salt Lake City, Utah) outputting close to 100 mW of optical power at 830 nm was utilized. Spectrograph system was a *f*/1.8i (Holospec, Kaiser Optical Systems). Tissue models and *in vitro* samples were imaged. Another IFP (Figure 18, right side) is seen in Komachi *et al*. [52], where an 8x1 fibre (SF112 UV, Japan) bundle was employed, where a fibre core with 114 µm in diameter was used. A Ti:Sapphire, background-free, electronically tuned laser outputting ~7 mW of optical power at 720 nm was also used. The spectrograph system was a UV-visible-near-IR spectrometer (UV 3100PC, Shimadzu Company, Kyoto, Japan). An array of biological samples where tested with this probe.

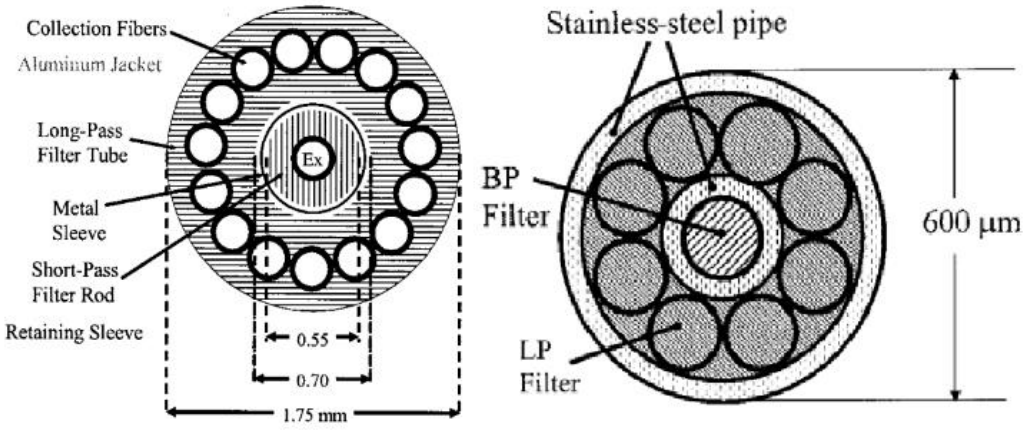

Figure 18. Schematics of Internally Filtered Probes (IFP). Left: A 15x1 geometry fibre bundle with a short-pass filter added on delivery fibre and long-pass filters to the collection fibres, adapted from [51]; Right: A 8x1 fibre bundle with long-pass and bandpass filters added to the collection and delivery fibres, adapted from [52].

A different system from an endoscopic one was described by Ashok *et al*. [53], where a microfluidic Raman probe inserted on a polydimethylsiloxane (PDMS) chip was built. A single delivery and collection fibres of low HO (Polymicro Technologies, AZ, USA) with 200 µm in diameter were used. A diode laser (Laser2000, (UK) Ltd.) outputted up to 200 mW maximum of optical power at 785nm and the signal was analysed in a spectrometer (Shamrock SR-303i, Andor Technology). The PDMS chip was fabricated with conventional soft lithographic techniques. Urea was measured and influence of flow on count rate was tested with ethanol.

Saar *et al*. [54], described a Raman fibre endoscopy probe that used both Stokes and pump beams. A single-mode polarization-maintaining fibre was used (PM780-HP, Thorlabs). The laser utilized was a mode locked Nd:YVO_4 laser at 1064 nm with 7 ps pulses with repetition rate of 80 MHz. Part of the laser output was frequency doubled and synchronously pumped by an optical parametric oscillator (Levante Emerald, APE GmbH), which generated a tuneable 800 nm pump beam. Signal acquisition was done with a photodetector and lock-in amplifier. Mouse tissue samples were analysed with this probe.

A.2 Endoscopy using Photonic crystal fibres

Photonic crystal fibres (PCF) where first discovered in the 1990's [55]. They differ from solid silica fibres by having air channels etched into them. The periodicity of the aligned air holes provides a confinement of light on the fibre core. There are reports of

many types of PCF, only two of them will be subject of analysis on this dissertation, namely: conventional solid core PCF [56] and hollow core photonic crystal fibres (HC-PCF) [57-64]. Solid core PCF (Figure 19. a)) are micro structured fibres where there is a solid silica core and the micro structured cladding of silica and air holes diminishes the surrounding overall refractive index, guiding light trough the silica core. On the other hand, HC-PCF (Figure 19. b), c)) are characterized by having an air core and a periodic structure in the cladding that acts as a Bragg reflector, being then a true photonic crystal, confining light to the hollow core by photonic bandgap guiding (PBG). The earliest works reporting usage of HC-PCF for Raman spectroscopy date back to 2002-2006 [56, 57].

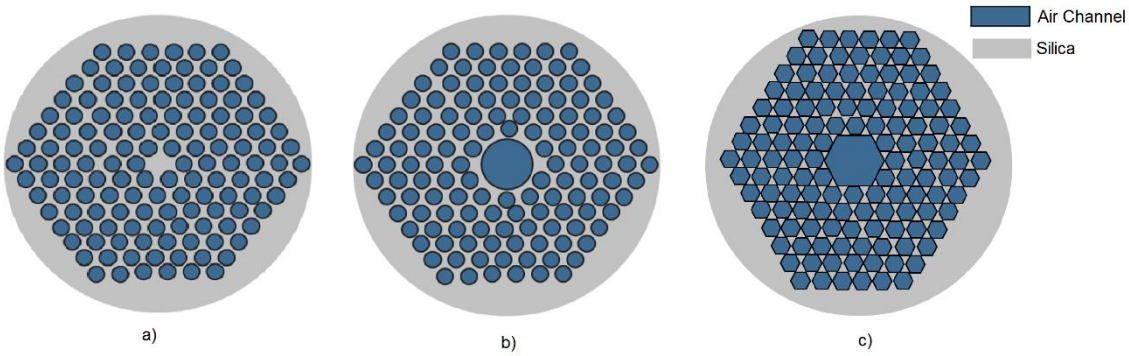

Figure 19. a) Solid core PCF; b) HC-PCF; c) Kagomé Lattice HC-PCF.

Benabid *et al*., [57] is one of the earliest works, in 2002. In it, a 1m long Kagome lattice HC-PCF with 15 µm core diameter was built. The fibre was filled with hydrogen gas and pumped with a Q-switched single-mode frequency-doubled Nd:YAG laser that operated at 532 nm with 6 ns pulses and 20 Hz repetition rate. Stokes and coherent anti-Stokes generation threshold and also pump-to-Stokes conversion efficiency was observed and analysed. Followed by Pristinski *et al*., [56]., that used a micro structured solid core fibre with a 2.5 µm silica core, with 126 3.5 µm air holes. A custom-made stainless-steel chamber facing fused silica windows sealed the fibre ends. The total probe length was of 0.2667 m. Coupled to it was a continuous wave Argon-ion laser that emitted 8mW of optical power at 488 nm. A neat acetonitrile solution filled the microstructure air holes and was analysed with a spectrometer with <100 ms of exposition time. On the same year Konorov *et al*. [58], a HC-PCF with 19 air holes was utilized, the fibre had an outer diameter of 84 µm, was 0.30 m long and with high transmission near 532 nm. The laser (Verdi V-10 Coherent) emitted 50 mW of optical power at 532 nm. The collection fibre was a standard silica core fibre, with 400 µm outer diameter and was 0.50 m in length. A spectrometer (Model 2061) was used to analyse Raman spectra of ethanol 95%(w/w).

In 2010, Balu *et al*. [59], tested three different fibres to deliver laser pulses. A single mode fused silica (HI 780, Corming), with a mode field diameter of ~4.8 µm and 0.40 m long, the second was a double clad PCF (A/S DC-165-16 PASSIVE, Crystal Fibre) mode field diameter of ~16 µm and 0.80 m long, the third was a large mode area PCF (LMA-20, Crystal Fibre) mode field diameter of ~20 µm and 0.5 m in length. For collection a multi-mode fibre (M28L01, ThorLabs) with 400 µm in core diameter and 1 m long was utilized. The laser system for the pump beam was a Ti:Sapphire oscillator, with 280 fs pulses at 76 MHz and 817 nm with 35 mW optical power. Stokes beam was generated by a mode locked laser source with 7.5 ps pulses at 76 MHz and 1064 nm with 25 mW optical power. A spectrometer (USB 4000 - VIS - NIR Miniature) monitored the output spectrum of each delivery fibre and a photomultiplier tube (R7400U-20, Hamamatsu) collected the signal. Images of adipocytes of fresh sample mouse ear (CD1/CD7 black wild), rabbit skin (Pathogen free, New Zealand) and lipid distribution of meibomian gland and eyelids of 2-month-old mice in 2% paraformaldehyde and PBS were generated with 512x512 pixels at 2 s per frame.

The year after, Brustlein *et al*. [60], employed a pure silica HC-PCF with 7 cells (air holes) counting the core, 2260 μm^2 was the collection cross section, with 200 nm width of air cladding struts, a diameter of 103 µm and with low loss from 950 nm to 1150 nm. The pump beam was produced from an optical parametric oscillator tuned from 962 nm to 971 nm, outputting 100 mW while the Stokes beam originated in a mode locked Nd:YVO with 7 ps pulses at 1064 nm with 100 mW. An avalanche photodiode detector (APD, Hamamatsu C5460) and a fast lock in amplifier were used to analyse spectra. The objective was to demonstrate coherent anti-Stokes Raman scattering and stimulated Raman scattering in an “endoscope-like” scheme using a double-clad hollow core photonic crystal fibre.

A 7 cell HC-PCF is also used by Khetani *et al*. [61], the fibre had 10.6 µm core diameter (+- 1 µm), a clad channel diameter of 3 µm (+- 1 µm) and was 0.10 m long. A laser diode with a central wavelength of 785 nm and 100 mW optical power was used. Together with a *f*/1.8*i* (Holospec, Kaiser Optical Systems) spectrometer system a pressure driven flow system was built and ethanol and isopropanol in concentrations from 5% to 60% in deionized water were analysed.

Other research groups [62-64] developed, studied and utilized a Kagomé lattice HC-PCF in a Raman spectroscopy endoscope. On a first stage [62] a 1.5 m long with undisclosed specifications Kagomé lattice HC-PCF (Figure 21. a)) was used and coupled to a He-Ne laser at 632.8 nm delivering 6 mW of optical power. The laser was coupled

to the fibre by a 150 mm lens with numerical aperture of 0.02 (same as fibre) and then focused onto a 1 cm quartz cuvette by 2 achromatic doublets with 25 mm in focal length. A dichroic mirror separated Raman scatter light from reflected and elastically scattered one (Omega 650 DRLP) plus a long pass filter (Omega 640 AELP) and bandpass filter (Kaiser Optics HNF-632.8-1.0). Spectrometer was a Horiba JobinYvon iHR320 with a Peltier-cooled CCD camera. Each spectrum consisted of 4 acquisitions of 10 seconds each. Schematic of the system is present in Figure 20.

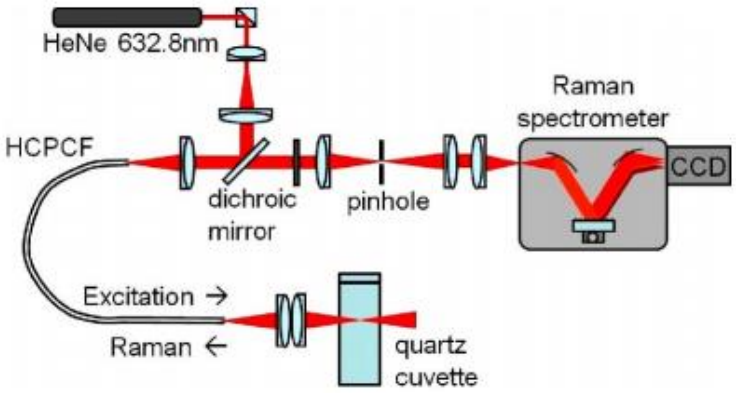

Figure 20. Schematic of Raman spectroscopic system. Adapted from [62].

Following it, a single mode Kagome lattice HC-PCF was utilized [63], specifications of the fibre are disclosed as being 278 µm in diameter with a 20µm wide core, the laser source ranged from 780 nm to 815 nm at around 200 mW of optical power. The objective was confirming the presence of parasitic signals and search parameters that are parasitic signal free. In the end [64], a Raman endoscope was built by using a double clad Kagomé lattice HC-PCF (Figure 21. b)). The fibre had an outer diameter of 327 µm and a core diameter of 20 µm wherein light propagated in a single transverse mode. A 30 µm microsphere was introduced to reduce laser spot on incident surface, from ~15 µm to ~1 µm, enabling high-resolution nonlinear imaging. Laser source for pump and Stokes beams was obtained from a tuneable multi-wavelength laser system (Discovery, Coherent) that provided two pulse trains at 80 MHz. The pump beam was at 800 nm and 100 fs wide while Stokes beam was at 1040 nm and 160 fs wide. Coherent anti-Stokes Raman Scattering (CARS), Second harmonic generator (SHG) and two-photon excited fluorescence (TPEF) images were built and displayed in real time using custom LabVIEW software based on an open-loop image reconstruction

algorithm with submicron spatial resolution over a field of view of up to 320 µm at a rate of 0.8 frames per second.

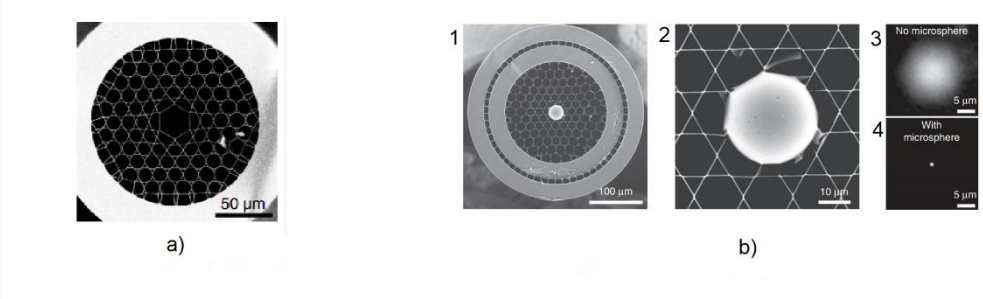

Figure 21. Scanning electron micrograph of fibre utilized a), adapted from [62]; b) 1: scanning electron micrograph of single mode, double clad Kagomé lattice HC-PCF, 2: close up image of microsphere utilized, 3 and 4: laser spot images without microsphere and with added microsphere, adapted from [64].

Closing Remarks

Raman spectroscopy using optical fibres is being researched for some time, with the major contribution using mono mode fibres being from the period of 1995 – 2000. The major advancements when using mono mode fibres would have to be, in my opinion, the fibre bundle configuration increasing the collecting area without increasing as much the complexity and the development of internal filtered probes, that helped to diminish signal noise while also miniaturizing more the probing apparatus.

Afterwards, Raman spectroscopy studies started using micro structured fibres. Namely PCF, HC-PCF and Kagomé lattice fibre. This type of fibres have high collecting area and their structure acts as a filter. While also having the advantage of being a single fibre.

If pursuing to develop a Raman spectroscopy system with portability in mind or with the ability for being applied in a clinical environment, basing on the research done the remarks would be: using 785nm excitation wavelength, it appears to be a suitable wavelength as seen in the works of Bergholt *et al*. [16, 20, 22, 27], and others; a double-clad Kagomé or HC-PCF fibre with either internal filtering or a filtered tip coupled to the fibre to reduce parasitic signal coming in and out of the probe; the Raman signal collected would be divided into two bands, being the first from 800-1200cm^{-1} and the second from 1200-1800cm^{-1} due to signal inversion around this wavenumber. The possible fingerprint peaks to look for would be (in cm^{-1}): 1004, 1335, 1445, 1618 and 1655 for being recurring peaks across multiple works.

References

[1] C. V. Raman, "A new radiation," in Indian Journal of Physics, pp. 387-398, 1928.

[2] Robert W. Boyd. 2008. Nonlinear Optics, Third Edition (3rd ed.). Academic Press, Inc., Orlando, FL, USA.

[3] S. Saint-Jalm, Soliton-based fiber light sources for nonlinear spectroscopy and microscopy, (phD dissertation), pp. 69-76 (2014)., pp. 69-76.

[4] R. Manoharan, Y. Wang and M. S. Feld, “Histochemical analysis of biological tissues using Raman spectroscopy”, in Spectrochimica Acta Part A: Molecular and Biomolecular Spectroscopy, vol. 52, no. 2, pp. 215-249, February 1996.

[5] R. Manoharan, Y. Wang, N. Boustany, J.F. Brennan, J.J. Baraga, R.R. Dasari, J. Van Dam, S. Singer and M.S. Feld, “Raman spectroscopy for cancer detection: instrument development and tissue diagnosis”, in Proc. SPIE, Biomedical Optoelectronic Devices and Systems II, vol. 2328, pp. 128-132, 22 December 1994.

[6] I. A. Birtoiu, M I. Rusu, N. D. Becherescu-Barbu, B. A. Vitalaru, D. Togoe, M. Pascal, M. V. Udrea, B. Chiricuta, C. Rizea, A. Parau and C. E.A. Grigorescu, “Micro-Raman sectrscopy in the visible range: a tool for rapid investigation of mammary tumours”, in Romanian Reports in Physics, vol. 67, no. 4, pp. 1525-1536, 2015.

[7] J. Kneipp, T. B. Schut, M. Kliffen, M. Menke-Pluijmers and G. Puppels, “Characterization of breast duct epithelia: a Raman spectroscopic study”, in Vibrational Spectroscopy, vol. 32, no. 1, pp. 67-74, 5 August 2003.

[8] F. M. Lyng, D. Traynor, T. N. Q. Nguyen, A. D. Meade, F. Rakib, R. Al-Saady, E. Goormaghtigh, K. Al-Saad and M. H. Ali, “Discrimination of breast cancer from benign tumours using Raman spectroscopy”, in Plos One, vol. 14, no. 4, 14 February 2019.

[9] S. Rehman, Z. Movasaghi, A. T. Tucker, S. P. Joel, J. A. Darr, A. V. Ruban and I. U. Rehman, “Raman spectroscopic analysis of breast cancer tissues: identifying differences between normal, invasive ductal carcinoma and ductal carcinoma in situ of the breast tissue”, in Journal of Raman Spectroscopy, vol. 38, no. 10, pp. 1345-1351 2 July 2007.

[10] J. Surmacki, J. Musial, R. Kordek and H. Abramczyk, “Raman imaging at biological interfaces: applications in breast cancer diagnosis”, in Molecular Cancer, 12:48, 24 May 2013.

[11] C.-H. Liu, Y. Zhou, Y. Sun, J. Y. Li, L. X. Zhou, S. Boydston-White, V. Masilamani, K. Zhu, Yang Pu and R. R. Alfano, “Resonance Raman and Raman Spectroscopy for Breast Cancer Detection”, in Technology in Cancer Research and Treatment, vol. 12, no. 4, August 2013.

[12] K. Kong, F. Zaabar, E. Rakha, I. Ellis, A. Koloydenko and I. Notinghe, “Towards intra-operative diagnosis of tumours during breast conserving surgery by selectivesampling Raman micro-spectroscopy”, in Physics in Medicine & Biology, vol. 59, no. 20, pp. 6141-6152, 21 October 2014.

[13] D. Lazaro-Pacheco, A. M. Shaaban, S. Rehman and I. Rehman, “Raman spectroscopy of breast cancer”, in Applied Spectroscopy Reviews, 23 April 2019.

[14] I. A. Birtoiu, C. Rizea, D. Togoe, R. M. Munteanu, C. Micsa, M. I. Rusu, M. Tautan, L. Braic, L. O. Scoicaru, A. Parau, N. D. Becherescu-Barbu, M. V. Udrea, A. Tonetto, R. Notonier and C. E. A. Grigorescu, “Diagnosing clean margins through Raman spectroscopy in human and animal mammary tumour surgery: a short review”, in Interface Focus, vol. 6, no. 6, 6 December 2016.

[15] R. M. Munteanu, L.O. Scoicaru, M. Militaru, E. Gagniuc, C. Micsa, D Togoe , A B. Vitalaru, M.I. Rusu, M. Tautan, B. Chiricuta, M. V. Udrea, A Sonea, C-E-A. Grigorescu and A I. Birtoiu, “Comparison of benign and malignant mammary tumors in dogs trough Raman spectroscopy: two clinical cases” in Scientific Works. Series C. Veterinary Medicine, vol. LXIII, no. 2, pp. 85-90.

[16] M. S. Bergholt, W. Zheng, K. Lin, K. Y. Ho, M. Teh, K. G. Yeoh, J. B. Y. So and Z. Huang, "Raman endoscopy for in vivo differentiation between benign and malignant ulcers in the stomach," in The Analyst, vol. 135, no. 12, pp. 3162-3168, 12 October 2010.

[17] Z. Huang, S. K. Teh, W. Zheng, K. Lin, K. Y. Ho, M. Teh and K. G. Yeoh, "In vivo detection of epithelial neoplasia in the stomach using image-guided Raman endoscopy," in Biosensors and Bioelectronics, vol. 26, no. 2, pp. 383-389, 15 October 2010.

[18] S. Luo, C. Chen, H. Mao and S. Jin, "Discrimination of premalignant lesions and cancer tissues from normal gastric tissues using Raman spectroscopy," in Journal of Biomedical Optics, vol. 18, no. 6, p. 067004, 4 June 2013.

[19] J. Wang, K. Lin, W. Zheng, K. Y. Ho, M. Teh, K. G. Yeoh and Z. Huang, "Fiber-optic Raman spectroscopy for in vivo diagnosis of gastric dysplasia," in Faraday Discussions, vol. 187, pp. 377-392, 2016.

[20] M. S. Bergholt, W. Zheng, K. Lin, K. Y. Ho, M. Teh, K. G. Yeoh, J. B. Y. So and Z. Huang, "In Vivo Diagnosis of Esophageal Cancer Using Image-Guided Raman Endoscopy and Biomolecular Modeling," Technology in Cancer Research & Treatment, vol. 10, no. 2, pp. 103-112, 1 April 2011.

[21] L. M. Almond, J. Hutchings, C. Kendall, J. C. C. Day, O. A. C. Stevens, G. R. Lloyd, N. A. Shepherd, H. Barr and N. Stone, "Assessment of a custom-built Raman spectroscopic probe for diagnosis of early oesophageal neoplasia," in Journal of Biomedical Optics, vol. 17, no. 8, pp. 081421, August 2012.

[22] M. S. Bergholt, W. Zheng, K. Y. Ho, M. Teh, K. G. Yeoh, J. B. Y. So, A. Shabbir and Z. Huang, "Fiberoptic Confocal Raman Spectroscopy for Real-Time In Vivo Diagnosis of Dysplasia in Barretts Esophagus," in Gastroenterology, vol. 146, no. 1, pp. 27-32, January 2014.

[23] S. Duraipandian, W. Zheng, J. Ng, J. J. H. Low, A. Ilancheran and Z. Huang, "Simultaneous Fingerprint and High-Wavenumber Confocal Raman Spectroscopy Enhances Early Detection of Cervical Precancer In Vivo," in Analytical Chemistry, vol. 84, no. 14, pp. 5913-5919, 17 July 2012.

[24] M. A. Veenstra, O. Palyvoda , H. Alahwal, M. Jovanovski, L. A. Reisner, B. King, J. Poulik and D. M. Klein, "Raman Spectroscopy in the Diagnosis of Ulcerative Colitis," in European Journal of Pediatric Surgery, vol. 25, no. 1, pp. 56-59, 2015.

[25] D. Petersen, P. Naveed, A. Ragheb, D. Niedieker, S. F. El-Mashtoly, T. Brechmann, C. Kötting, W. H. Schmiegel, E. Freier, C. Pox and K. Gerwert, "Raman fiber-optical method for colon cancer detection: Cross-validation and outlier identification approach," in Spectrochimica Acta Part A: Molecular and Biomolecular Spectroscopy, vol. 181, pp. 270-275, 15 June 2017.

[26] P. C. Lopes, J. A. Moreira, A. Almeida, A. Esteves, I. Gregora, M. Ledinsky, J. M. Lopes, R. Henrique and A. Oliveira, "Discriminating adenocarcinoma from normal colonic mucosa through deconvolution of Raman spectra," in Journal of Biomedical Optics, vol. 16, no. 12, p. 127001, December 2011.

[27] M. S. Bergholt, W. Zheng, K. Lin, K. Y. Ho, M. Teh, K. G. Yeoh, J. B. Y. So and Z. Huang, "Combining near-infrared-excited autofluorescence and Raman spectroscopy improves in vivo diagnosis of gastric cancer," in Biosensors and Bioelectronics, vol. 26, no. 10, pp. 4104-4110, 15 June 2011.

[28] L. M. Almond, J. Hutchings, G. Lloyd, H. Barr, N. Shepherd, J. Day, O. Stevens, S. Sanders, M. Wadley, N. Stone and C Kendall, “Endoscopic Raman spectroscopy enables objective diagnosis of dysplasia in Barrett’s esophagus”, *in Gastrointestinal Endoscopy*, vol. 79, no. 1, pp. 37-45, January 2014

[29] K. Larsson and L. Hellgren, “A Study of the Combined Raman and Fluorescence Scattering from Human Blood Plasma”, *in Experientia*, vol. 30, no. 5, pp. 481-483, May 1974.

[30] S.P. Verma, D.F.H. Wallach, J.R. Philippot, M. Zanca and B. Bonnet. ‘‘Abnormal Raman Scattering by Plasma of Patients With Cancer’’, *in Journal of the National Cancer Institute*, vol. 78, no. 3, pp. 587-589, 1 March 1987.

[31] R. C. Clarke, Q. Wang and J. M. Isner, “Laser Raman spectroscopy of atherosclerotic lesions in human coronary artery segments”, *in Applied Optics*, vol. 27, no. 23, pp. 4799-4800, 1988.

[32] S. Saito, M. Tasuma and C.H. Eugster, “Resonance Raman Spectra (5800-40 cm^{-1}) of All-trans and 15=cis Isomers of p=Carotene in the Solid State in Solution. Measurements to and with Various Laser Lines from Ultraviolet Red”, *in Journal of Raman Spectroscopy*, vol. 14, no. 5, October 1983.

[33] C. Liu, B.B. Das, W.L.S. Glassman, G.C. Tang, K.M. Yoo, H.R. Zhu, D.L. Akins, S.S. Lubicz, J. Cleary, R. Prudente, E. Celmer, A. Caron and R.R. Alfano, “Raman, fluorescence, and time-resolved light scattering as optical diagnostic techniques to separate diseased and normal biomedical media”, *in Journal of Photochemistry and Photobiology B: Biology*, vol. 16, no. 2, pp. 187-209, 30 October 1992.

[34] A. Mizuno, Y. Hayashi, K. Tashibu, S. Muraishi, K. Kawauchi and Y. Ozaki, “Near-infrared FT-Raman spectra of the rat brain tissues”, *in Neuroscience Letters*, vol. 141, no. 1, pp. 47-52, 6 July 1992.

[35] A. Mizuno, H. Katajima, K. Kawauchi, S. Muraishi and Y. Ozaki, “Near-Infrared Fourier Transform Raman Spectroscopic Study of Human Brain Tissues and Tumours”, *in Journal of Raman Spectroscopy*, vol 25, no. 1, pp. 25-29, January 1994.

[36] M.S. Feld, R. Manoharan, J. Salenius, J. OrensteinCarndona, T.J. Romer, J.F. Brennan III, R.R. Dasari and Y. Wang, “Detection and characterization of human tissue lesions with near infrared Raman spectroscopy”, *in Proc. SPIE, Advances in Fluorescence Sensing Technology II*, vol 2388, 8 May 1995.

[37] S. Nie, K. J. Bergbauer, J. J. Ho, J. F. R. Kuck, Jr. and N. T. Yu, ‘‘Application of near-infrared Fourier transform Raman spectroscopy in biology and medicine,’’ *in Spectroscopy*, vol. 5, pp. 24–32, 1990

[38] R. Scott, C. Kendall, N. Stone and K. Roger, “Elemental vs. phase composition of breast calcifications”, *in Scientific Reports*, vol. 7, article: 136, 9 March 2017.

[39] M. C. Paoloni and C Khanna, “Comparative Oncology Today”, *in Veterinary Clinics of North America: Small Animal Practice*, vol. 37, no. 6, pp. 1023-1032, November 2007.

[40] F. Sultan and B. A. Ganaie, “Comparative oncology: Integrating human and veterinary medicine”, *in Open Veterinary Journal*, vol. 8, no. 1, pp. 25-34, 30 January 2018.

[41] D. M. Vail and E. Gregory Macewen, "Spontaneously Occurring Tumors of Companion Animals as Models for Human Cancer", *in Cancer Investigation*, vol. 18, no. 8, pp. 781-792, 2000

[42] Baba AI, Câtoi C. Comparative Oncology. Bucharest: The Publishing House of the Romanian Academy; 2007. Chapter 1, COMPARATIVE ONCOLOGY.

[43] M. L. Myrick, S. M. Angel and R. Desiderio, "Comparison of some fiber optic configurations for measurement of luminescence and Raman scattering," in Applied Optics, vol. 29, no. 9, pp. 1333-1344, 20 March 1990.

[44] A. J. Berger, Y. Wang, D. M. Sammeth, I. Itzkan, K. Kneipp and M. S. Feld, "Aqueous Dissolved Gas Measurements Using Near-Infrared Raman Spectroscopy," in Applied Spectroscopy, vol. 49, no. 8, pp. 1164-1169, 1 August 1995.

[45] A. J. Berger, Y. Wang and M. S. Feld, "Rapid, noninvasive concentration measurements of aqueous biological analytes by near-infrared Raman spectroscopy," in Applied Optics, vol. 35, no. 1, pp. 209-212, 1 January 1996.

[46] J. F. Brennan, Y. Wang, R. R. Dasari and M. S. Feld, "Near-Infrared Raman Spectrometer Systems for Human Tissue Studies," Applied Spectroscopy, vol. 51, no. 2, pp. 201-208, 1 February 1997.

[47] A. Mahadevan-Jansen, M. F. Mitchell, N. Ramanujam, U. Utzinger and R. Richards-Kortum, "Development of a Fiber Optic Probe to Measure NIR Raman Spectra of Cervical Tissue In Vivo," in Photochemistry and Photobiology, vol. 68, no. 3, pp. 427-431, September 1998.

[48] M. G. Shim and B. C. Wilson, "Development of an In Vivo Raman Spectroscopic System for Diagnostic Applications," in Journal of Raman Spectroscopy, vol. 28, no. 2-3, pp. 131-142, 4 December 1998.

[49] M. G. Shim, B. C. Wilson, E. Marple and M. Wach, "Study of Fiber-Optic Probes for in vivo Medical Raman Spectroscopy," in Applied Spectroscopy, vol. 53, no. 6, pp. 619-627, 1 June 1999.

[50] M. G. Shim, L.-M. W. K. Song, N. E. Marcon and B. C. Wilson, "In vivo Near-infrared Raman Spectroscopy: Demonstration of Feasibility During Clinical Gastrointestinal Endoscopy," in Photochemistry and Photobiology, vol. 72, no. 1, pp. 146-150, July 2000.

[51] J. T. Motz, M. Hunter, L. H. Galindo, J. A. Gardecki, J. R. Kramer, R. R. Dasari and M. S. Feld, "Optical Fiber Probe for Biomedical Raman Spectroscopy," in Applied Optics, vol. 43, no. 3, p. 542, 20 January 2004.

[52] Y. Komachi, H. Sato, K. Aizawa and H. Tashiro, "Micro-optical fiber probe for use in an intravascular Raman endoscope," in Applied Optics, vol. 44, no. 22, pp. 4722-4732, 1 August 2005.

[53] P. C. Ashok, G. P. Singh, K. M. Tan and K. Dholakia, "Fiber probe based microfluidic raman spectroscopy," in Optics Express, vol. 18, no. 8, pp. 7642-7649, 12 April 2010.

[54] B. G. Saar, R. S. Johnston, C. W. Freudiger, X. S. Xie and E. J. Seibel, "Coherent Raman scanning fiber endoscopy," in Optics Letters, vol. 36, no. 13, p. 2396, 1 July 2011.

[55] T. A. Birks, D. M. Atkin, T. J. Shepherd, P. S. J. Russell and P. J. Roberts, "Full 2-D photonic bandgaps in silica/air structures," in Electronics Letters, vol. 31, no. 22, pp. 1941-1943, 26 October 1995.

[56] D. Pristinski and H. Du, "Solid-core photonic crystal fiber as a Raman spectroscopy platform with a silica core as an internal reference," in Optics Letters, vol. 31, no. 15, pp. 3246-3248, 15 November 2006.

[57] F. Benabid, J. C. Knight, G. Antonopoulos and P. S. J. Russel, "Stimulated Raman Scattering in Hydrogen-Filled Hollow-Core Photonic Crystal Fiber," in Science, vol. 298, pp. 399-402, 11 October 2002.

[58] S. O. Konorov, C. J. Addison, H. G. Schulze, R. F. B. Turner and M. W. Blades, "Hollow-core photonic crystal fiber-optic probes for Raman spectroscopy," in Optics Letters, vol. 31, no. 12, pp. 1911-1912, 15 June 2006.

[59] M. Balu, G. Liu, Z. Chen, B. J. Tromberg and E. O. Potma, "Fiber delivered probe for efficient CARS imaging of tissues," in Optics Express, vol. 18, no. 3, pp. 2380-2388, 1 February 2010.

[60] S. Brustlein, P. Berto, R. Hostein, P. Ferrand, C. Billaudeau, D. Marguet, A. Muir, J. Knight and H. Rigneault, "Double-clad hollow core photonic crystal fiber for coherent Raman endoscope," in Optics Express, vol. 19, no. 13, pp. 12562-12568, 20 June 2011.

[61] A. Khetani, J. Riordon, V. Tiwari, A. Momenpour, M. Godin and H. Anis, "Hollow core photonic crystal fiber as a reusable Raman biosensor," in Optics Express, vol. 21, no. 10, pp. 12340-12350, 20 May 2013.

[62] P. Ghenuche, S. Rammler, N. Y. Joly, M. Scharrer, M. Frosz, J. Wenger, P. S. J. Russell and H. Rigneault, "Kagome hollow-core photonic crystal fiber probe for Raman spectroscopy," in Optics Letters, vol. 37, no. 21, pp. 4371-4373, 1 November 2012.

[63] A. Lombardini, E. R. Andersen, A. Kudlinski, I. Rimke and H. Rigneault, "Origin and suppression of parasitic signals in Kagomé lattice hollow core fibers used for SRS microscopy and endoscopy," in Optics Letters, vol. 42, no. 9, pp. 1824-1827, 1 May 2017.

[64] A. Lombardini, V. Mytskaniuk, S. Sivankutty, E. R. Andresen, X. Chen, J. Wenger, M. Fabert, N. Joly, F. Louradour, A. Kudlinski and H. Rigneault, "High-resolution multimodal flexible coherent Raman endoscope," Light: Science & Applications, vol. 9, no. 1, 30 May 2018.